AIM OF THE WORK

The aim of this work is to evaluate the role of antibacterial nanofibers by incorporating silver nanoparticles into nanofibers using electrospinning as wound dressing on excisional wound healing dynamics in diabetic mice in comparison with physical methods such as ultrasound and laser treatments.

MATERIALS AND METHODS

I- Preparation of Nanomaterials

1- Preparation and characterization of silver nanoparticles

2- Preparation and characterization of cellulose acetate nanofibers

3- Preparation and characterization of silver loaded cellulose acetate nanofibers

II- Nano-therapies for Wound Healing

I. Preparation of Nanomaterials:

I.1.1 Preparation of silver nanoparticles:[206]

a- Materials

AgNO3 ($AgNO_3$, 99.99%) and trisodium citrate dihydrate ($C_6H_5O_7Na_3.2H_2O$, 99.99%), were purchased from Sigma Aldrich. Deionized water.

b- Method

Silver nanoparticles were synthesized according to the method of Zhou and Wang (2012). Briefly, 10 mL of $AgNO_3$solution (5mM) in deionized water was heated until it began to boil, then 1 mL trisodium citrate solution (1%) was added drop wise; heating continued until the color was changed to pale yellow. The solution was cooled to room temperature. The growth of nanoparticles is monitored by UV-vis spectrophotometer and complemented with characterization using Transmission Electron Microscopy, X-ray Diffraction analysis

I.1.2 Characterization of silver nanoparticles

a- UV-Visible spectrum analysis

UV-Visible (UV-Vis) absorption spectroscopic measurements were recorded on a single beam spectrophotometer (UNICAM UV-Vis spectrometry model UV5-220) Figure (13), using quartz cell of 1 cm path length and deionized water as the reference solvent at room temperature. A UV-Vis spectrum is an indication of Surface Plasmon Resonance (SPR) that depicts the size and distribution of nanoparticles

Fig. 13: UV-Vis spectrophotometer (UNICAM UV-Vis spectrometry model UV5-220)

b- XRD (X-ray Diffraction*)* analysis

After the complete reduction of silver nanoparticles the solution was lyophilized using lyophilizer (Telestar –Spain) and the dried mixture was analyzed for the crystalline nature of Ag nanoparticles by X-ray diffractometer (Shimaduz, XRD- 7000, Maxima, Japan) operated at operated at a voltage of 30 KV and a current of 30 mA with CuKα radiation and analyzed between 5 and 100^{o} (2 θ), Figure (14).

Fig.14: X-ray diffractometer (Shimadzu, XRD-7000, Maxima, Japan)

c- Transmission Electron microscope (TEM):

Transmission electron microscopy (TEM) images of the Ag NPs were taken with transmission electron microscope (JEOL-100 CX) Figure (15). The samples for TEM measurements were prepared by placing a droplet of the colloidal solution onto a carbon coated cupper grid and allow it to dry in air naturally at room temperature.

Fig.15: Transmission Electron Microscopy (JEOL-100 CX, Japan).

I.2.1 preparation of Cellulose acetate nanofibers loaded Ag nanoparticles: [207, 208]

a- Materials

Cellulose Acetate (CA, Mw = 61,000 g/mol, acetyl content of 40%), Acetone (98%), N,N-dimethylformamide [DMF] and $AgNO_3$ ($AgNO_3$, 99.99%) were purchased from Sigma Aldrich.

b- Method

A polymer solution of 15% (w %) of CA was prepared by dissolving CA in a mixture solvents of acetone and DMF (2:1 v/v). The mixture was then mechanically stirred using a magnetic stirrer at room temperature for 3 hours to form a homogeneous solution. For preparation of CA nanofibers containing Ag NPs, different percentage 1%, 3% and 5% $AgNO_3$ was thoroughly mixed into the polymer solution.

The solution was immediately collected into a 10 ml syringe equipped with a 24 gauge stainless steel needle tip. CA nanofibers were prepared using the electrospinning technique in an air-conditioned laboratory. The process conditions were kept at an ambient temperature of 22^{o}C and relative humidity of <65%.

The syringe was fixed on an electric syringe pump set to maintain a constant feed rate of 1 ml/h. A high-voltage power supply (Gamma high voltage, Inc., USA) was employed to apply positive charge to the needle, and a grounded metal plate covered with aluminum foil served as the collector. The voltage used for electrospinning was 20 kV.

The distance between the needle tip and collector was 15 cm. The nanofibers was leaved to dry then it was characterized. CA nanofibers containing $AgNO_3$ were exposed to UV irradiation at 245 nm for 1 h to reduce silver ions in the nanofibers to silver nanoparticles. Figure (16) shows the image of the electrospinning experimental set up at Medical Biophysics Department, MRI.

Electrospining process

In the electrospinning process the syringe is filled with the polymer solution. When a high voltage is applied, usually in the range of 1-30 kV, the polymer solution becomes electrified. A droplet at the tip of the syringe needle, when electrified, experiences two types of electrostatic forces- the electrostatic repulsion between the surface charges and the Columbic force by external electric field.

Under these forces, the drop is drawn out into a Taylor cone. Once the electrostatic forces overcome the surface tension of the polymer solution, the electrified jet undergoes stretching and bending, eventually forming into a continuous filament. As this process continues, the solvent from the polymer solution evaporates thereby solidifying the fiber.

This fiber is deposited onto a collector which is grounded. The diameter of the deposited fiber can be controlled through electrospinning parameters like solution viscosity, applied voltage, distance between the syringe needle tip and collector surface and many others. The positive electrode from the high voltage source was connected to the spinneret tip by means of an alligator clip. The negative terminal of the power source and the collector screen were grounded as show in figure (17).

Cellulose acetate nanofibers had been prepared by using binary solvent system investigated the relationship between cellulose acetate solution properties and morphology of nanofibers, included that a mixture of acetone/dimethylformamide (2:1) was electrospun into nonwoven fiber mesh.

Fig.16: Photograph of the Electrospinning laboratory set up.

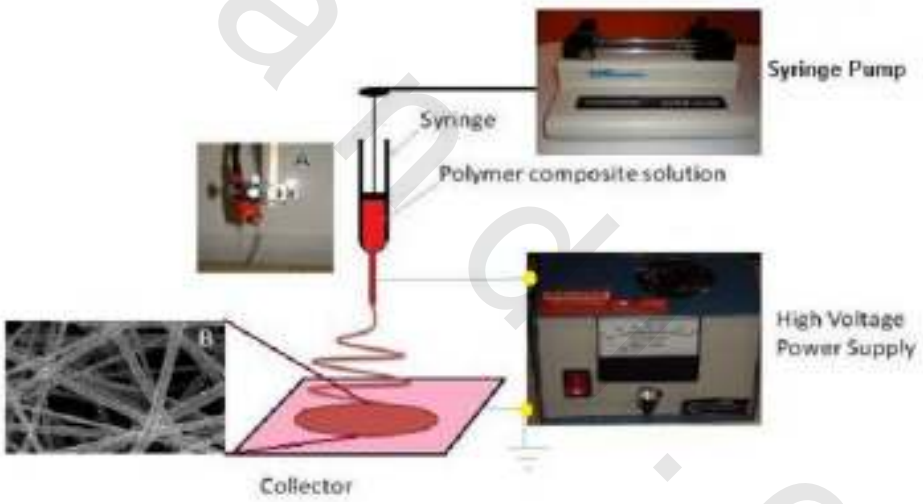

Fig. 17: Schematic diagram of the complete electrospinning setup. A) Needle connected to the high voltage power supply. B) Nanofibrous mats.

I.2.2Characterization of CA Nanofibers and silver loaded CA nanofiber

a- Scanning Electron Microscope (SEM)

After forming the nanofibers web onto the aluminum collector, the structure and the morphology of nanofibres spun were characterized by using Scanning Electron Microscopy (SEM, JEOL-5300) Figure (18). In order to view non-conductive samples, the sample were coated with a thin layer of gold using ion sputtering device (JEOL JEC-1100E) Figure (19).

The sputtering device coats the sample with 10 μm thickness gold atoms. The purpose is to make non-metallic samples electrically conductive to be detected by SEM. The average diameter of the nanofibers was determined by measuring and imaging the diameter of random nanofibers.

Fig.18: Scanning Electron Microscopy SEM (JEOL-5300, Japan).

Fig.19: SPI- module TM Sputter coater.Japan.

b- Fourier transforms infrared spectrophotometer

Fourier transforms infrared (IR) spectroscopy measures the absorption of IR radiation by materials as the atoms vibrate about their bonds. It is primarily used to identify bond types, structures and functional groups in organic and inorganic compounds. IR sensitive vibrations are associated with changes in dipole moments.

Fourier transforms infrared spectroscopy measures vibrational energy levels in molecules. It can be used for both qualitative and quantitative analysis, to identify molecules and compounds, and to determine the presence or absence of certain types of bonds and functional groups.

For example, double and single bonds associated with carbon-hydrogen and carbon oxygen bonding (=C-H,-C-H, C-O and C=O) can be distinguished by IR absorption.

When functional groups can be bonded at different locations on molecules, IR spectroscopy can frequently identify the positions at which the functional groups are attached. The reason is that vibrational frequencies differ when functional groups are attached at different sides in molecules.

When illuminated by IR radiation of the appropriate frequencies, atoms, ions, and functional groups in molecules will vibrate about their bonds and energy will be absorbed. Each bending and stretching vibrational mode of a molecule or functional group will absorb at a particular frequency. When exposed to appropriate IR frequencies, energy will be absorbed from the incident radiation as vibrational intensities increase. Many IR frequencies have no effect at all and will not be absorbed.

IR characterization of CA nanofibers and Ag coated nanofibers were performed with FT-IR spectrophotometer (Alpha-centauri) (Shimadzu, Japan, FT-IR-8400S) (Figure.20) with a frequency range of 4000-400 cm^{-1}. CA Nanofibers and silver coated nanofibers prepared in the forms of potassium bromide (KBr) disk.

Approximately 40-60 mg of powder and 120 mg of KBr was blended and triturated with agate mortar and pestle for 10 min. Approximately 40 mg of the mixture were compacted using a IR hydraulic press at a pressure of 8 tons for 60 s. The disk was conditioned in a desiccator placed in an oven at 80°C for 16 hr before analysis.

The spectra of samples (in the forms of KBr disk) were obtained with a frequency range of 4000-400 cm^{-1}

Fig. 20: Fourier transforms infrared spectrophotometer

c- Dispersion X-Ray analysis (EDX):-

Energy Dispersive X-Ray Analysis (EDX), referred to as EDS or EDAX, is an x-ray technique used to identify the elemental composition of materials. Applications include materials and product research.

EDX systems are attachments to SEM and TEM instruments where the imaging capability of the microscope identifies the specimen of interest. The data generated by EDX analysis consist of spectra showing peaks corresponding to the elements making up the true composition of the sample being analyzed.

The compositional and elemental analysis of the prepared Ag loaded nanofibers were carried out by EDX combined with the scanning electron microscopy.

d- Antibacterial Activity of Silver loaded nanofibers against *Staphylococcus aureus* and *Escherichia coli* using different concentration of silver coated nanofiber [207, 209]

1. Determining the antibacterial activity of silver-loaded nanofiber against *Staphylococcus aureus* and *Escherichia coli* in comparison to free nanofibers and different classes of antibiotics using Disc diffusion method:

Reagents for the Disc Diffusion Test

a) Müller-Hinton Agar Medium (Oxoid®)

Müller-Hinton Agar was prepared from dehydrated base according to the manufacturer's instructions.

b) Antibiotic Discs (Oxoid®)

The antibiotic discs were stored in refrigerator (2 - 8° C)

c) Nanofibers with different concentrations (1,3,5 %) of Ag loaded CA nanofibers and a free nanofiber as a control.

d) Turbidity standard for inoculum preparation

To standardize the inoculum density for a susceptibility test, a BaSO4 turbidity standard equivalent to a 0.5 McFarland standard was used.

Procedure for Performing the Disc Diffusion Test

- The Kirby-Bauer method was used for antimicrobial susceptibility testing.
- The inoculum was prepared using direct colony suspension method by making a saline suspension of isolated colonies selected from 18-24 hour blood agar plates of *Staphylococcus aureus* and *Escherichia coli*.

Inoculation of Test Plates

1) Within 15 minutes after adjusting the turbidity of the inoculum suspension, a sterile cotton swab was dipped into the adjusted suspension. The swab was rotated several times and pressed firmly on the inside wall of the tube above the fluid level. This removed excess inoculum from the swab.

2) The dried surface of a Müller-Hinton agar plate was inoculated by streaking the swab over the entire sterile agar surface. This procedure was repeated by streaking two more times, rotating the plate approximately 60° each time to ensure an even distribution of inoculum. As a final step, the rim of the agar was swabbed.

3) The lid was left open for 3 to 5 minutes, but no more than 15 minutes, to allow for any excess surface moisture to be absorbed before applying the drug impregnated discs.

4) The selected antimicrobial discs from different classes were dispensed onto the surface of the inoculated agar plate. Each disc was pressed down to ensure complete contact with the agar surface. The discs were placed individually. They were distributed evenly so that they were no closer than 24 mm from center to center.

5) Nanofibers with different concentrations (1, 3, 5%) of Ag loaded CA nanofibers and a free nanofibers as control were dispensed onto the surface of the inoculated agar plate in the same way as antimicrobial discs.

6) The plates were inverted and placed in an incubator set to 37°C within 15 minutes after the discs are applied.

Reading Plates and Interpreting Results

- After 24 hours of incubation, each plate was examined. The diameters of the zones of complete inhibition (as judged by the unaided eye) were measured, including the diameter of the disc and the nanofibers.
- Zones were measured to the nearest whole millimeter, using a ruler, which was held on the back of the inverted Petri plate. The Petri plate was held a few inches above a black, nonreflecting background and illuminated with reflected light.

2- Determining the growth curves of bacterial cells exposed to different concentrations of silver loaded nanofibers

1- Nutrient broth medium was prepared by dissolving 28 gm of nutrient agar in 1000 ml of distilled water. The above solution was autoclaved subsequently at 121^{o}C, for 30 min.

2- Fresh colonies of *Escherichia coli* and *Staphylococcus aureus* were cultured into nutrient broth containing flasks and the bacterial cell concentration was adjusted to approximately 10^5 colony forming units (CFU)/ml

3- Nanofiber with different concentrations (1, 3, 5%) of Ag loaded CA nanofibers were added to the culture flasks.

4- Silver-free nutrient broth containing flasks were cultured under the same conditions and used as a control.

5- Each culture was incubated in a shaking incubator at 37^{o}C for 24 h.

6- Growth curves of bacterial cell cultures were attained through repeated measures (at 2,4,6,12,24 hours of inoculation) of the optical density (OD) at 600 nm using (Unicam UV5-220) spectrophotometer.

7- After 24 hours of incubation, cultural broth and nanoparticle solution was observed for turbidity.

II. Nanotherapies for wound healing of mice in comparison to physical treatment

1- Experimental animals (70 mice):

Laboratory Swiss albino mice of either, 6-8 weeks of age, weighing 25-30 g were obtained from the animal house of MRI. The animals were allowed to acclimatize for 2 weeks before experiment. The animals were housed in polyethylene cages inside a well-ventilated room. Each cage was not containing more than 5 mice. The mice will be maintained under standard laboratory conditions of temperature and humidity and 12 hour light /dark cycle.

2- Induction of diabetes mellitus: [210]

1- Diabetes was induced with a single intra peritoneal (i.p.) injection of Streptozetocin (Sigma) STZ with a dose 180 mg/kg body weight, after a fasting period of 12 hours.

2- STZ was dissolved in cold 0.1 M citrate buffer, pH 4.5 and always prepared freshly for immediate use within 5 min to avoid degradation of STZ.

3- The doses determined according to the body weight of animals. Every STZ dose dissolved in 0.5 ml of citrate buffer pH 4.5 and given intra peritoneal to the mouse.

4- After injection of STZ, the mouse allowed to awaken and placed back in cage. This procedure was repeated for each animal. Mice were supplied with 10% sucrose water, if necessary, to avoid sudden hypoglycemia post-injection.

5- Blood glucose levels were determined by a drop of blood obtained from the cut tail vein and measuring with the glucose monitoring system (FREE STYLE FREEDOM LITE). If the blood glucose level is >300 mg/dl, the animal considered to have successful induction of diabetes and were used in the study. All induced mice were treated with insulin intraperitoneally with a dose of 5 IU/kg.

3- Excision wound model:

Animals were anaesthetized prior to and during creation of the wounds. The dorsal fur of the animals was shaved with an electric clipper, and the anticipated area of the wound to be created was outlined on the back of the animals with methylene blue using a circular stainless steel stencil. A full thickness of the excision wound of circular area 95 mm^2 and 2 mm depth was created along the markings using toothed forceps, a surgical blade and pointed scissors, the entire wound was left open. Wounded mice were randomly divided into the following groups:

Group (I): Diabetic free served as control group (10 mice) injected with citrate buffer.

Group (II): Experimental group (60 mice) injected with Streptozotocin, this group were divided into the following subgroups:

IIa- Experimental group (10 mice), their open wounds left without treatment.

IIb- Experimental group (10 mice), their open wounds treated with Ag NPs only (50µL every other day).

IIc- Experimental group (10 mice), their open wounds dressed with CA nanofibers only.

IId- Experimental group (10 mice), their open wounds dressed with CA nanofibers loaded Ag NPs.

IIe- Experimental group (10 mice) treated with insulin combined with laser (650 nm, 150 mW) with a fluence of 5 J/cm^2 5 minutes daily, for 10 days, Figure (21).

IIf- Experimental group (10 mice) treated with insulin combined with pulsed ultrasound (0.5 W/cm^2) 5 minutes daily, for10 days, Figure (22).

4- Exposure Conditions

a. Laser apparatus: [211]

Laser phototherapy was done using low energy diode laser (Photon Co) with average power of (5 J/cm^2), the laser probe was directed over the animal wound with a distance apart 0.6 cm for 5 minutes daily 5 days/ week until complete healing, Figure (21).

Fig. 21: Laser source device (650 nm, 150 mW).

b. Ultrasonic apparatus

Ultrasonic therapy instrument (Ultrasonic Therapy Model CSL,Shanghai, No.822 factory, China) was used. This instrument uses calcium zirconate titanate circular transducer which operates at frequency of 0.8 MHz continuous- wave (CW) mode with output power from 0.5 to 3 W (average intensity 0.5 W/cm^2) adjustable in 11 steps at pulsed mode with adjustable power of 0.5 W (pulse- repetition rate 1000 Hz, duty ratio 1:3 and average intensity 0.5 W/cm^2). Transducers were mounted on a brass holder cooled with water. Figure (22).

Ultrasound therapy: [77]

After wound surgery, the treatment was started in group within 2 hours of the surgical procedure. The ultrasonic therapy treatment protocol include: Standard cleaning of wound by alcohol, Sterile coupling gel was put onto the wound and filled the wound cavity then Sterile plastic drape was applied to the wound and surrounding tissues to prevent any cross-contamination of the device. (The plastic drape should overlap wound margins by at least 5 cm).The sterile coupling gel was applied again on plastic drape and over wound area.

Pulsed ultrasonic therapy (applicator 1.9 cm^2) was applied over plastic drape and moved within the wound boundaries. Power density for group was 0.5 W/cm^2. Moving of

ultrasonic applicator was done for 5 minutes per day, day after day, five treatments per week until complete healing. Gel and plastic drape were removed and, wounds in all three groups were cleaned, dried at the end of each session.

Fig. 22: pulsed ultrasound (0.5 W/cm^2)

5- Experimental observation

The wound closure rate was assessed by tracing the wound every other day using transparency paper and a permanent marker. The rate of contraction (healing) was calculated. [212]

$$H.F = \frac{initial\ wound\ area - final\ wound\ area}{initial\ wound\ area} * 100$$

6- Histological evaluation: [213]

1- 3 mice from each group were sacrificed on the 4th, 10th and 15th days after surgery.

2- Skin wounds were removed and kept in formalin till processed routinely for light microscopy.

3- Two sections from each wound were made and stained with hematoxylin-eosin (HE – basic staining) and Masson trichrome respectively.

7- Mechanical properties measurements

After complete healing, Full-thickness of healed skin was used for biomechanical evaluation using tensile testing machine (Force meter BG500, USA Mark-10) as in Figure (23) (a). A sample was spaced between the jaws of the machine and stretched to failure.

Figure (23) (b): shows schematic diagram of the system used for measurement of the mechanical properties of the skin. To measure the thickness of the skin strips' an electronic micrometer (Micro 2000, Moore & Wright, and Sheffield, UK) was used. Tensile testing machine (Force meter BG500, USA) was used to stretch the strips, using 10 mm of their length at both ends to clamp them to the machine.

A sample was spaced 11 mm between the jaws they were located and stretched to failure by the tensile testing machine and the mechanical properties (stress and strain) was measured.

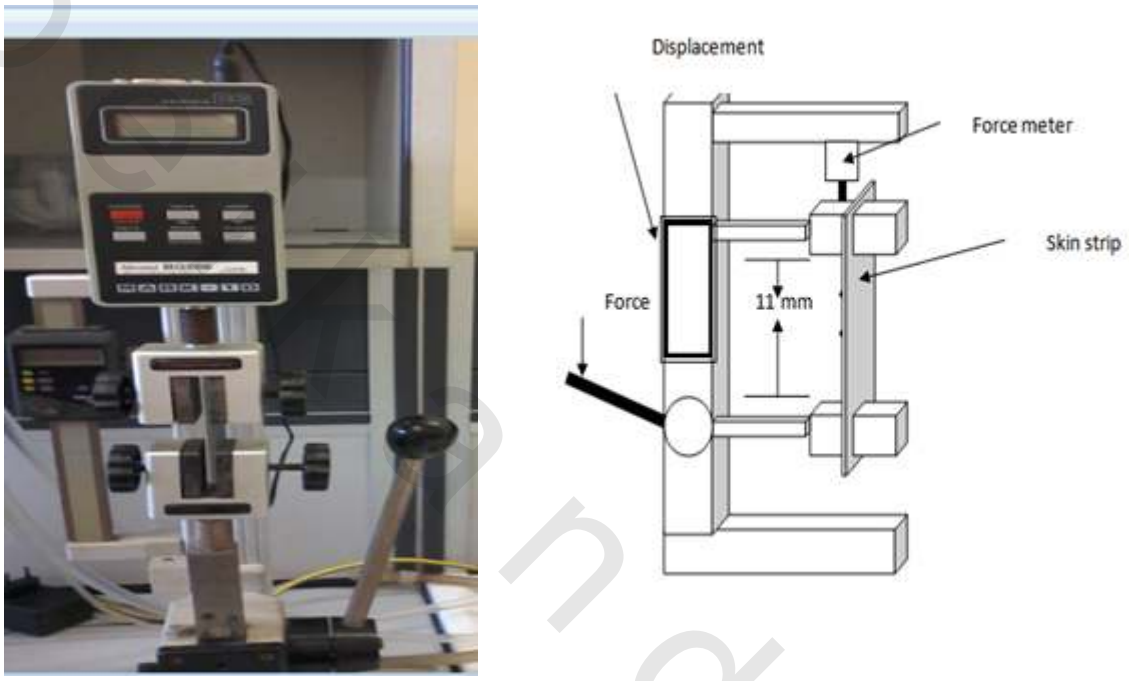

(a) **(b)**

Fig. 23: Machine and Schematic diagram of the system used for measurement of the mechanical properties of the skin, (a) and (b) respectively.

RESULTS

I. Characterization of Silver Nanoparticles

I.1 UV-Visible spectrum analysis

Figure (24) illustrates the UV-Vis absorption spectra of the Ag NP synthesized by the reduction of silver nitrate with tri-sodium citrate. The UV-Vis absorption spectra of Ag NPs showed surface Plasmon band occurs at around 430 nm indicating the presence of spherical Ag NPs.

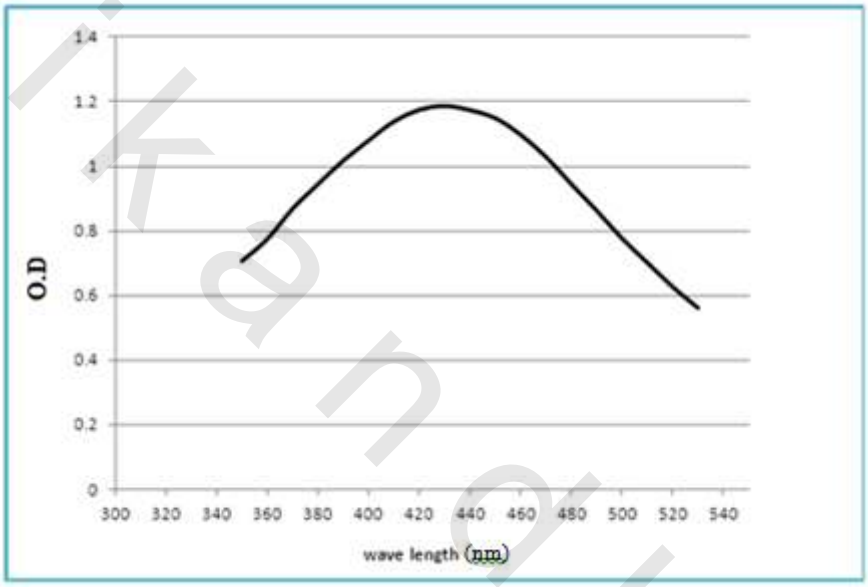

Fig. 24: The UV-Vis absorption spectra of the Ag NP.

I.2 TEM Images

The typical TEM micrographs of the synthesized Ag nanoparticles are presented in Figure (25). It is observed that most of the Ag nanoparticles were spherical in shape and homogeneously distributed. There is a variation in particle sizes ranging from 4.32nm to 7.27 nm with an average size 5.79 nm.

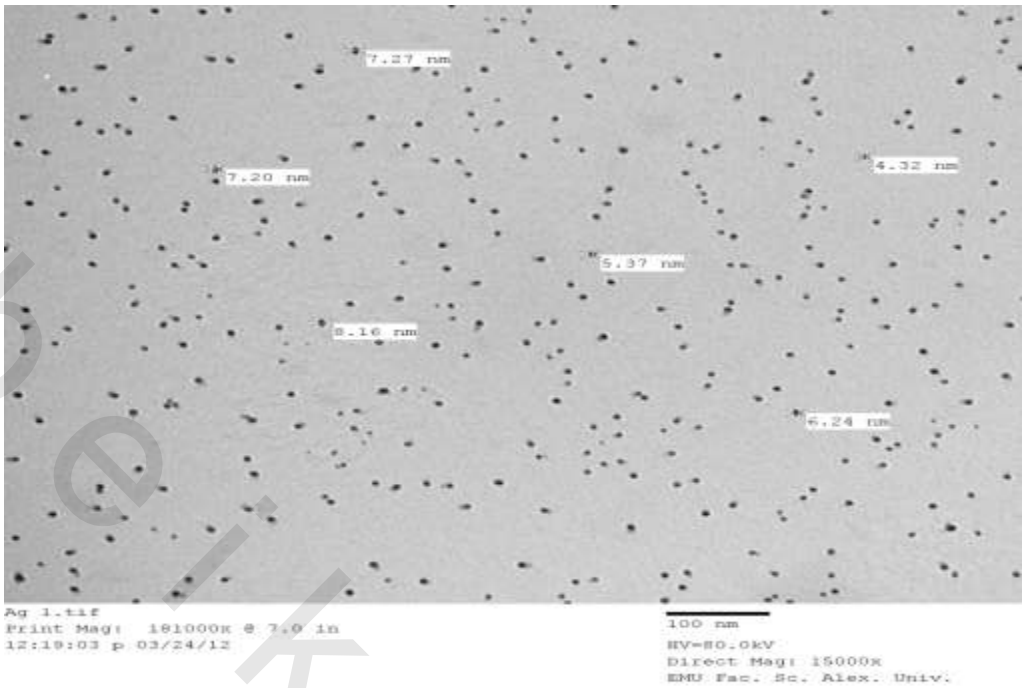

Fig. 25: TEM images and corresponding size distribution of silver nanoparticles.

I.3 Confirmation of Ag NPs by X-ray diffraction:

The XRD pattern of Ag-NPs is shown in Figure (26), three prominent peaks at 38° (2θ) and 42^{o} (2θ) and 68^{o}(2θ) indicated the presence of (111), (200) and (220) sets of lattice planes and further on this basis of they can be indexed as face-centered–cubic structure of Ag NPs.

Hence from the XRD pattern it is clear that silver nanoparticles were essentially crystalline in nature. The average crystalline particles size for Ag NPs determined by Scherre's formula using the half width of the most intense X-ray diffraction peaks was 4.17$\pm$1.12 nm. It can be noted that the size of the Ag nanoparticles obtained from TEM is in good agreement with the size obtained from the XRD measurements.

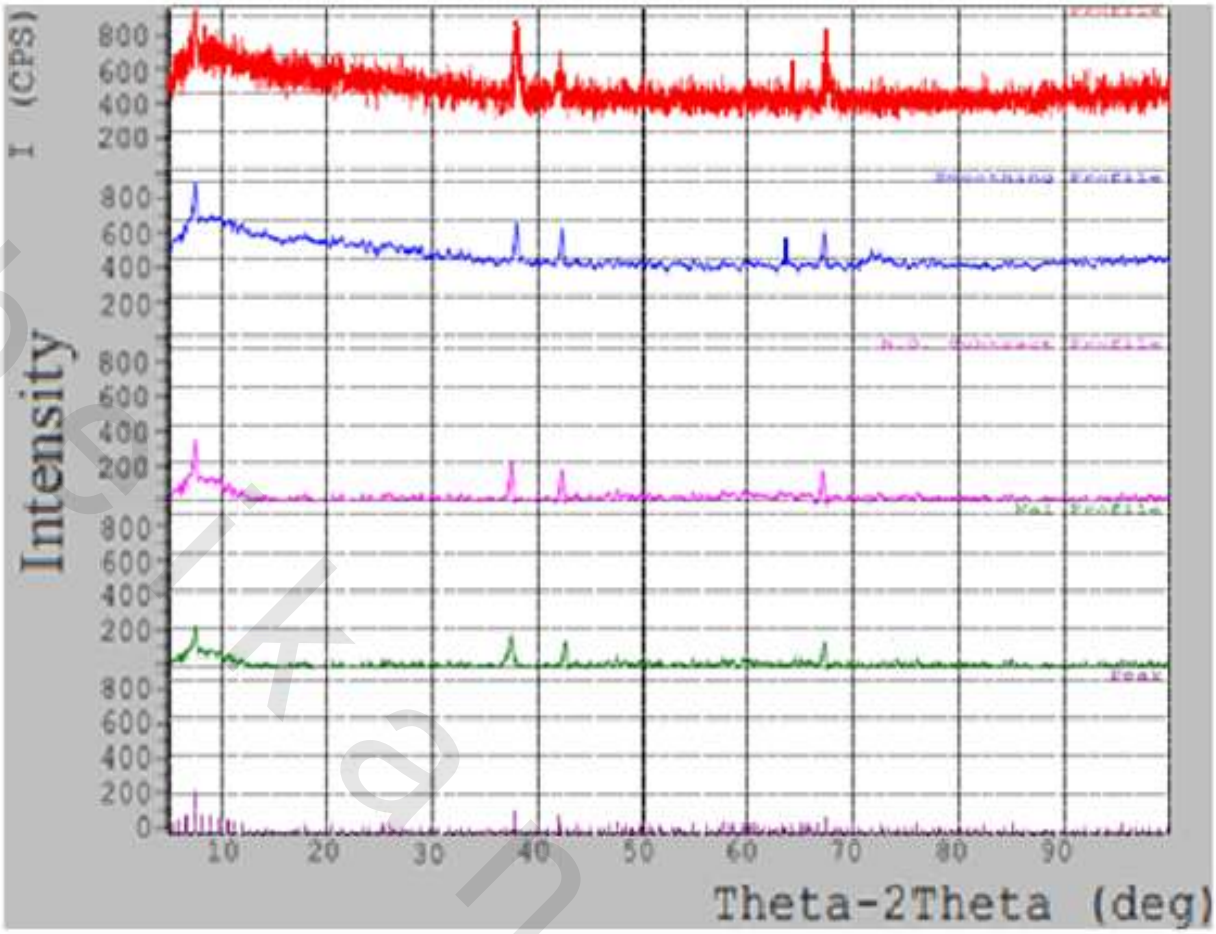

Fig. 26: X- ray diffraction spectrum of silver nanoparticles using tri-sodium citrate.

A: Profile obtained from XRD

B: Smoothing for curve profile

C: Subtraction of background from curve profile

D: Ka1- a2 separate

II. Characterization of CA nanofibers and Ag coated Nanofiber

II.1 Characterization of CA nanofibers containing silver nanoparticles with SEM and EDX:

Geometric properties of nanofibers such as fiber diameter, diameter distribution, fiber orientation and fiber morphology (e.g. cross-section shape and surface roughness) was characterized using scanning electron microscopy (SEM). Figure (27) showed the morphological structures of the electrospun (15 weight %) cellulose acetate products with binary solvents system (acetone/DMF, 2:1 w/w). Figure (28) and (29) respectively showed morphological structures and the EDX analysis of the CA nanofibers with silver

nanoparticles, a distinctive energy peak at around 3 keV, characteristic of silver was shown.

Good quality nanofibers with smooth surface were obtained as proved by the SEM images presented in Figure (27). The morphology of the nanofibers shown in (28) suggest that addition of silver nitrate to CA solution resulted in an increased solution conductivity and caused a slight decrease of fibers diameter, the presence of Ag NPs make the surface of nanofibers rough, as shown at high magnification (35,000X). The EDX analysis of the CA nanofibers loaded with silver nanoparticles shows a distinctive energy peak at around 3 keV, characteristic of silver as shown in figure (29).

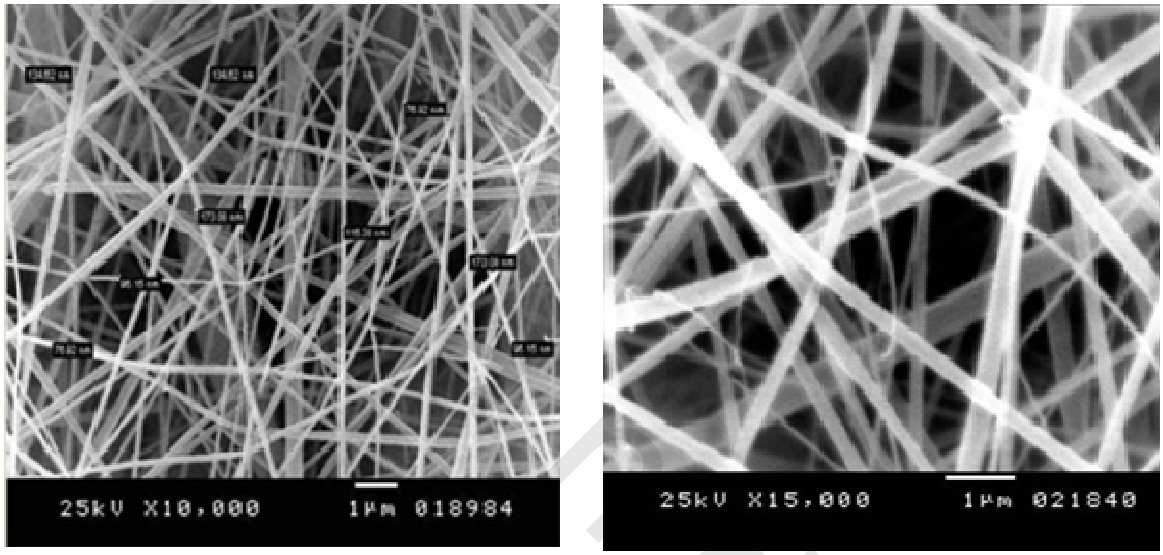

Fig. 27: SEM of CA nanofibers at different magnification.

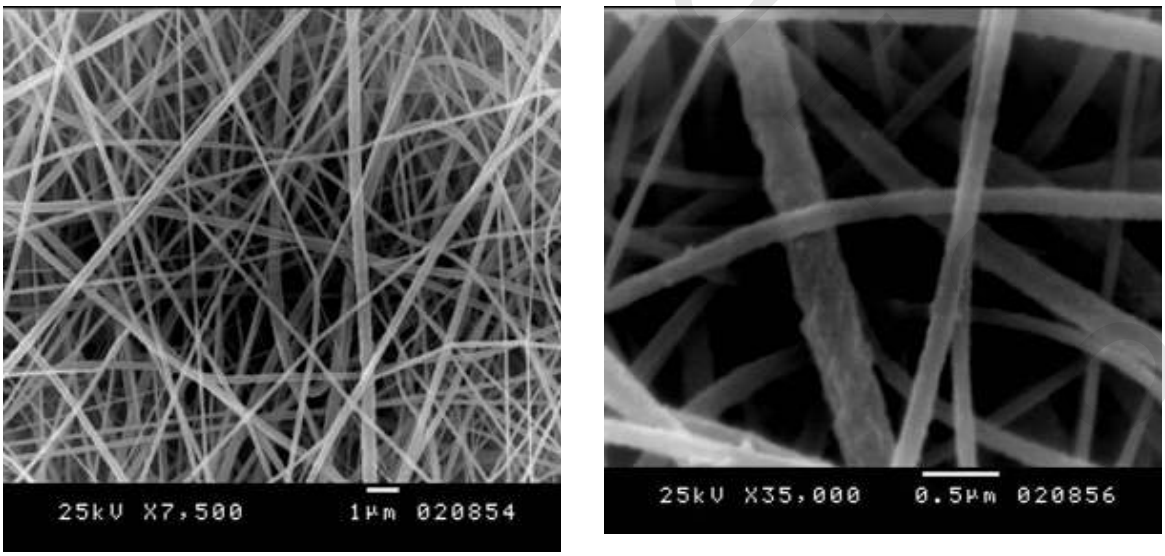

Fig. 28: SEM of CA nanofibers loaded with Ag nanoparticles .

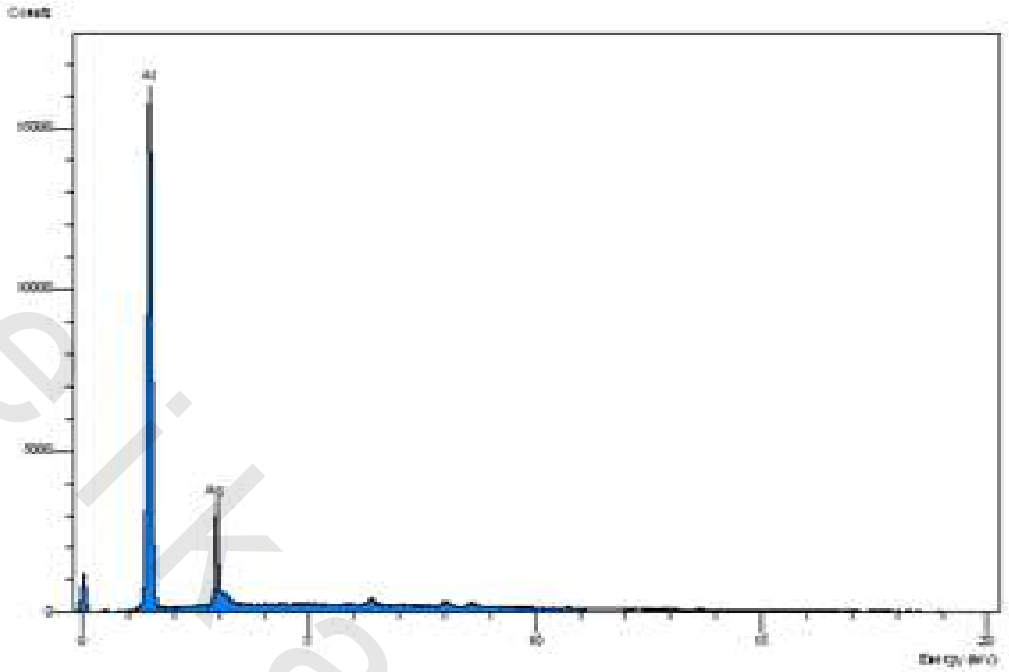

Fig. 29: EDX spectrum of silver loaded in CA nanofibers.

II.2 FTIR of cellulose acetate nanofibers:

Figure (30) and (31) showed Fourier-transform Infrared spectra for CA nanofibers and CA nanofibers loaded with Ag NPs respectively. CA nanofibers showed two strong absorption bands at 1745cm^{-1}and 1245cm^{-1}, which attributed to the C=O stretching and the acetyl groups, respectively. The adsorption band at 1633cm^{-1}was assigned to the water adsorption, the peaks at 1380, 1245 cm^{-1} are due to the aliphatic CH group vibrations of different modes CH, CH_2 and CH_3.

Another peak at 2926 cm^{-1} is due to the stretch vibration of methylene group (CH_2). The band at 3425 cm-1 corresponds to O-H stretching. As illustrated there are no major difference between the two samples in the major peak bands .However, it is also seen that the intensities of some peaks increase, this can be attributed to the presence of Ag NPs. The absorption peak at 2922 cm^{-1}, suggest that the silver nanoparticles caused a reordering of CA chains by promoting the formation of peptide CH_2 links.

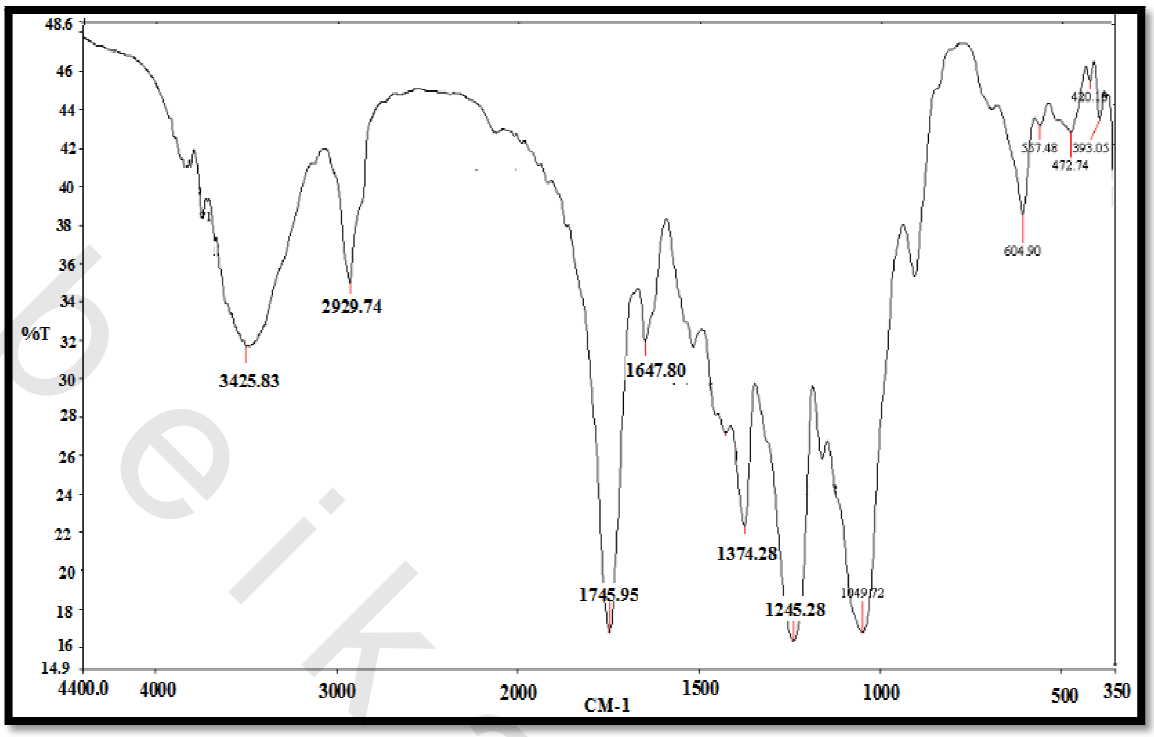

Fig. 30: FTIR of cellulose acetate nanofiber

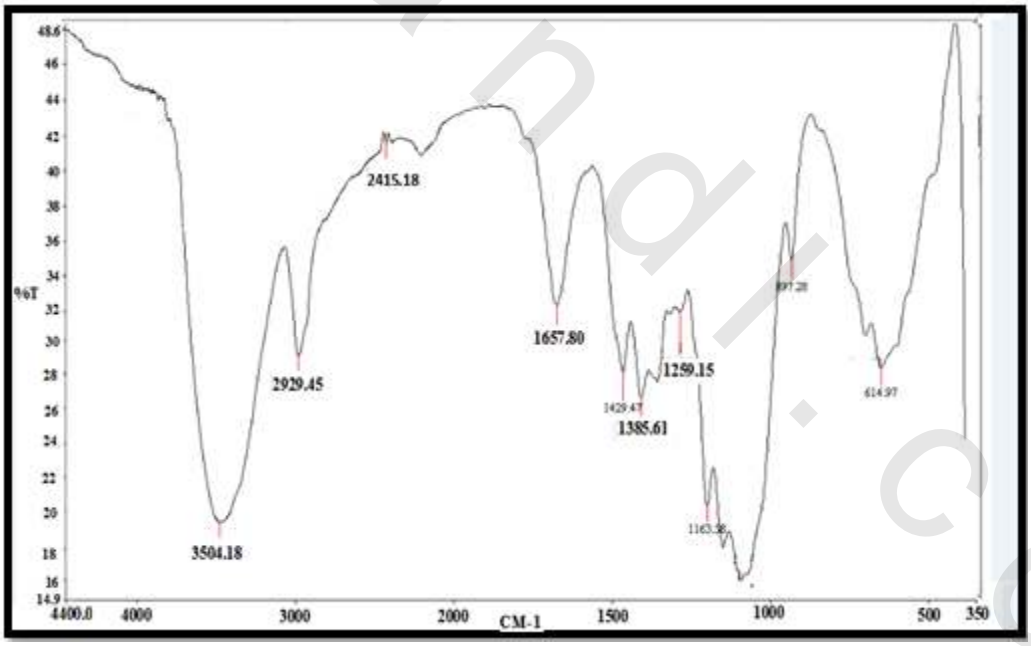

Fig. 31: FTIR of silver loaded cellulose acetate nanofiber.

II.3 Anti-bacterial activity of CA nanofibers loaded with silver nanoparticles

1- Disc Diffusion test:

Antibacterial effect of CA nanofiber loaded with Ag NPs was studied against two different pathogenic bacteria; Gram positive *Staphylococcus aureus* and Gram negative *Escherichia coli* strains.

Figures (32) and (33) show 24 h incubated petri dishes of *E. coli* and *S. aureus* grown in presence of circular nanofiber disk. From these Figures we can clearly observe the inhibition zones around the circular nanofiber disks containing different percentages of silver (1, 3 and 5%), while as in case of pure CA (0%) nanofibers and standard antibiotics like Gentamycin and Ciprofloxacin (ABC), these inhibition zones were missing, which confirms the antibacterial property of CA loaded with Ag NPs against bacteria resistant to antibiotics. It is clear from the Figures that the antibacterial activity increased (zone of inhibition) as the silver loaded on nanofibers increased.

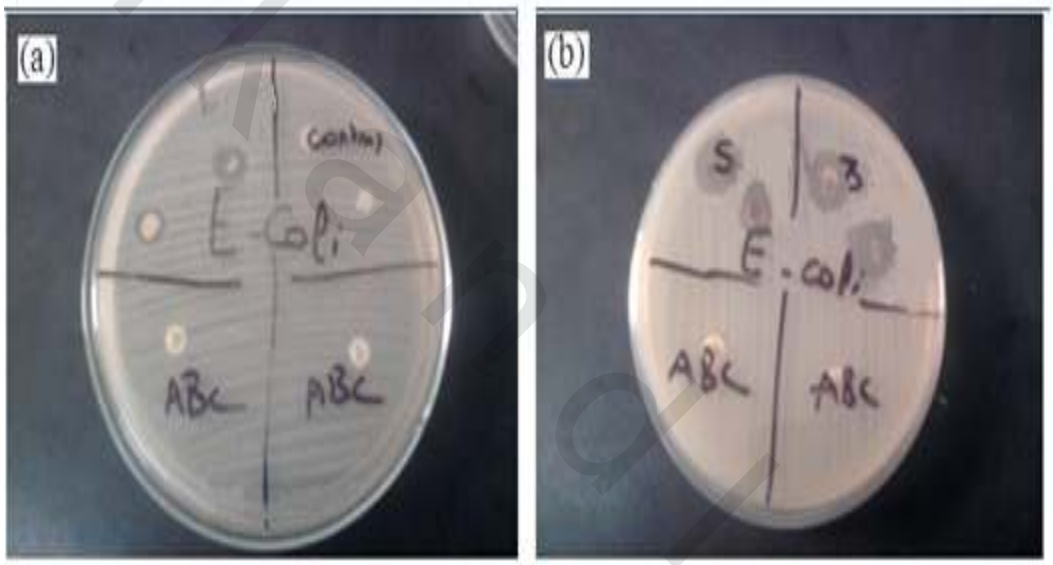

Fig. 32: Agar plates showing zones of inhibitions after 24 h of incubation with CA nanofibers loaded with different concentration of Ag NPs nanoparticles (0, 1, 3, 5 %) and other antibiotics Gentamycin, and Ciprofloxacin (ABC) for *E. coli* (a and b).

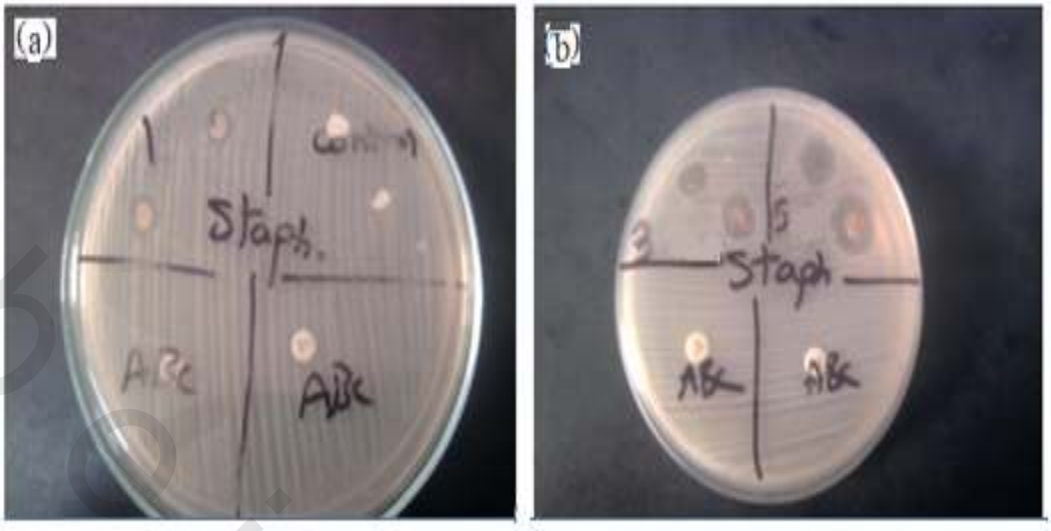

Fig. 33: Agar plates showing zones of inhibitions after 24 h of incubation with CA nanofibers loaded with different concentration of Ag NPs nanoparticles (0, 1, 3, 5 %) and other antibiotics Gentamycin, and Ciprofloxacin (ABC) for *S. aureus* (a and b).

2- Growth kinetics study

The synthesized CA NFs loaded with various concentrations of Ag nanoparticles were administered to *E. coli* and *S. aureus* to investigate the growth behavior of bacteria.

For *E. coli,* From the Figures (34) to (39) and table (1) also For *E. coli,* From the Figures (40) to (45) and table (2) it was noticed that, as the concentration of Ag NPs increased the growth inhibited.

This clearly indicates that Ag NPs produced toxicity to *E.coli* and *S. aureus*. Nanofibers loaded with 5% Ag NPs was found to have highest toxicity to the bacteria.

A- Growth kinetics study for *E.Coli*.

Table (1): Growth kinetics study for *E-Coli* using CA nanofibers loaded with different concentrations of Ag NPs.

Ag w% / Time (hour)	Optical Density (O.D)			
	Control (0%)	1%	3%	5%
0	0.124±0.015	0.124±0.015	0.124±0.015	0.124±0.015
2	0.18±0.017	0.093±0.016	0.077±0.012	0.067±0.014
4	0.25±0.025	0.081±0.015	0.061±0.014	0.05±0.016
6	0.35±0.027	0.066±0.016	0.042±0.013	0.032±0.017
8	0.382±0.031	0.051±0.017	0.033±0.011	0.021±0.013
10	0.391±0.033	0.04±0.017	0.02±0.012	0.017±0.012
12	0.41±0.036	0.03±0.015	0.018±0.001	0.008±0.001

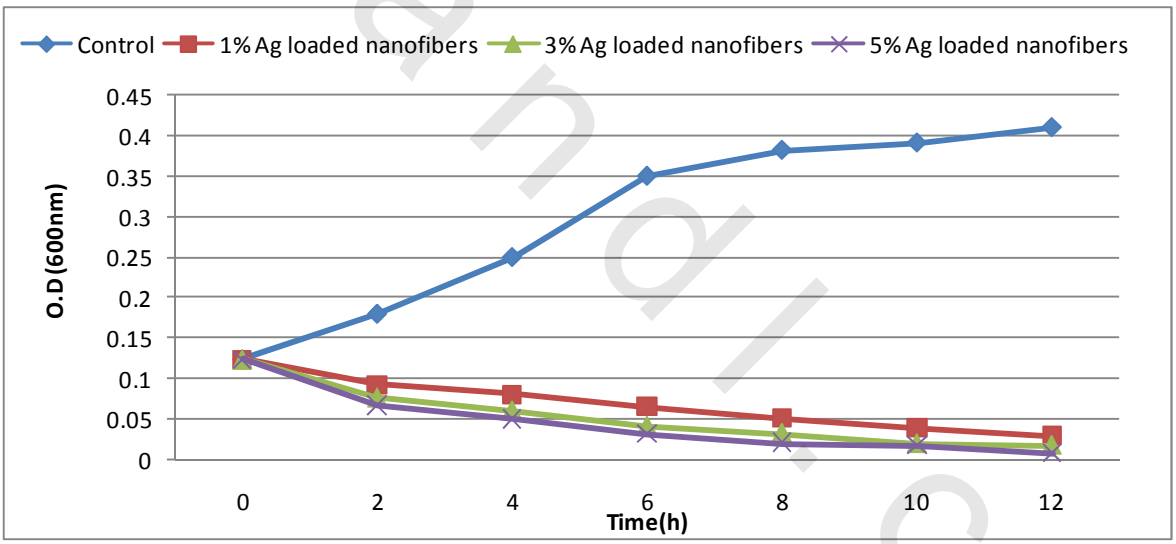

Fig. 34: The effect of Ag loaded nanofibers with different concentrations on the growth of *E. Coli*.

Table (2): Zone of Inhibition of Antibacterial Test of CA nanofibers loaded with Ag NP for *E-Coli.*

Ag (w %)	Zone of inhibition (Diameter, cm)
0	0
1	1.35±0.04
3	1.85±0.05
5	1.9±0.05

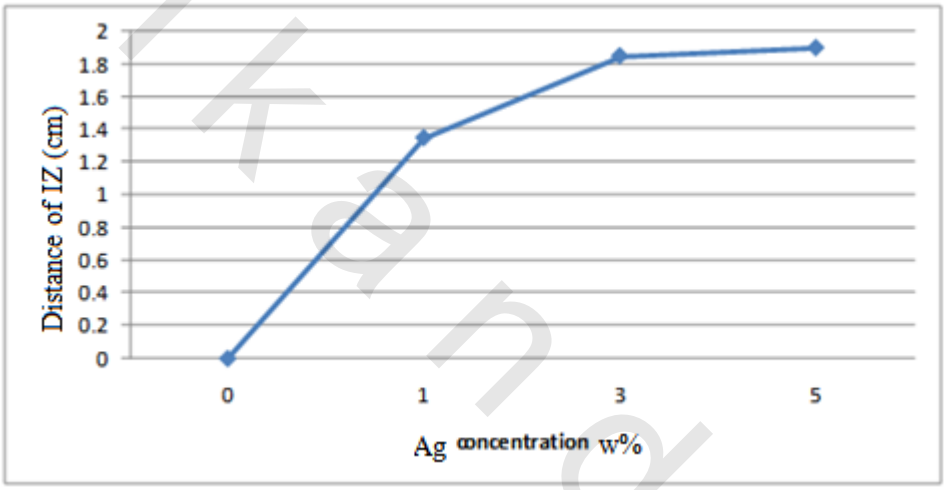

Fig. 35: Shows the effect of different concentration of silver loaded nanofiber on *E-Coli* by plotting the diameter of the inhibition zone of bacterial growth against the concentration of silver nanoparticles.

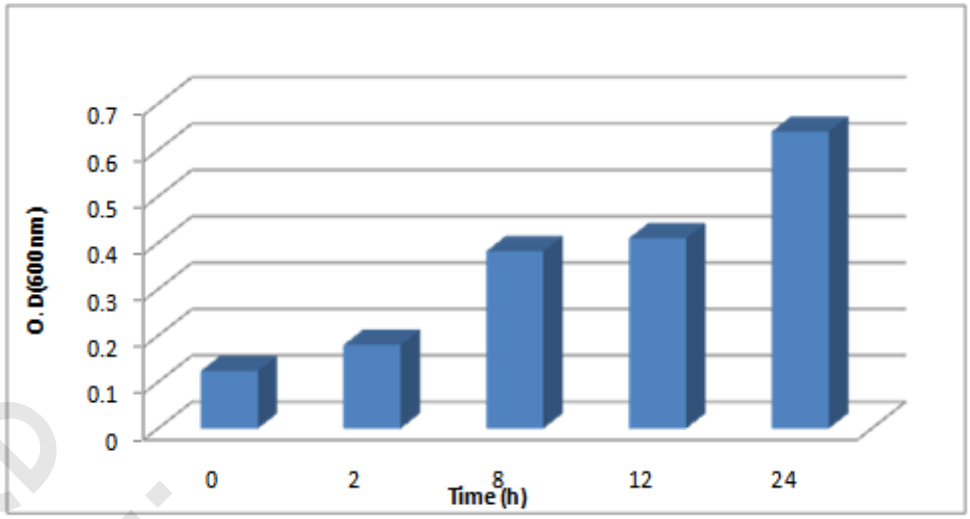

Fig. 36: Shows the effect of CA nanofiber on growth kinetic of *E-Coli* though 24 hours.

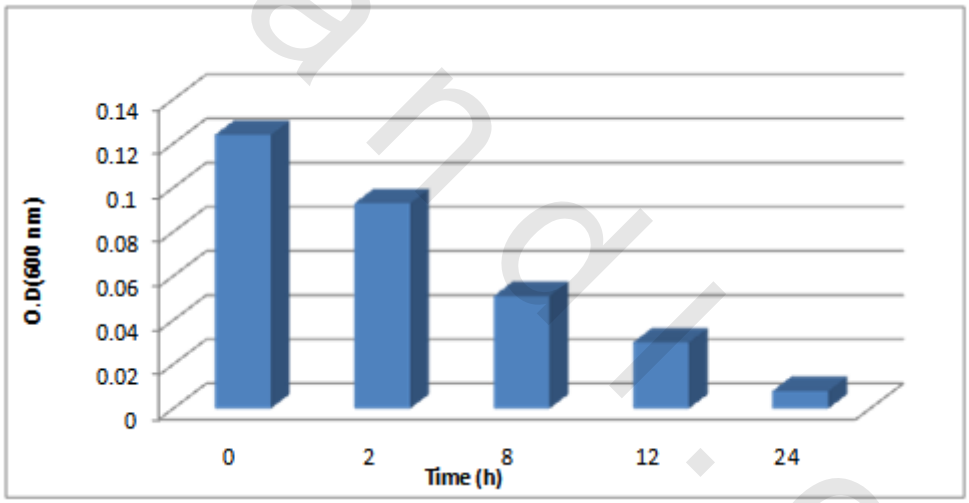

Fig. 37: Shows the effect of CA nanofiber loaded with Ag NPs (1w%) on growth kinetic of *E-Coli* though 24 hours.

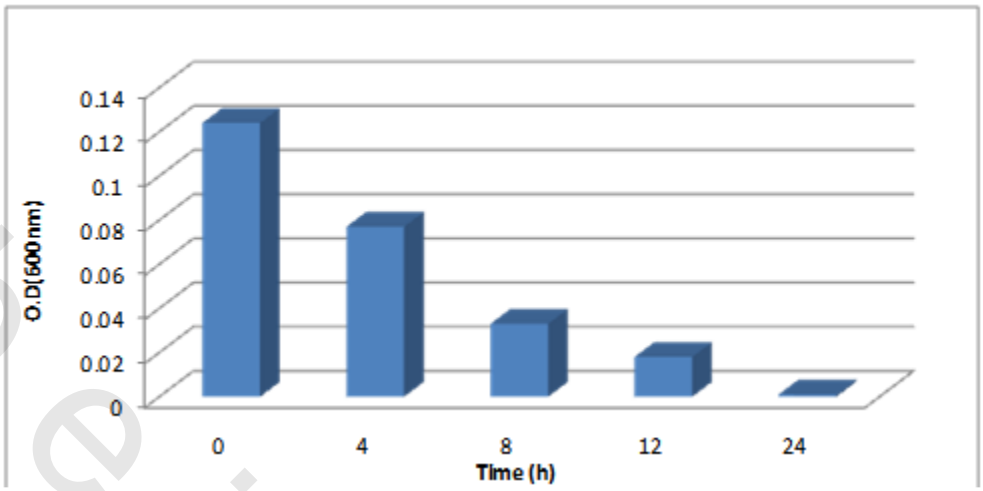

Fig. 38: Shows the effect of CA nanofiber loaded with Ag NPs (3w%) on growth kinetic of *E-Coli* though 24 hours.

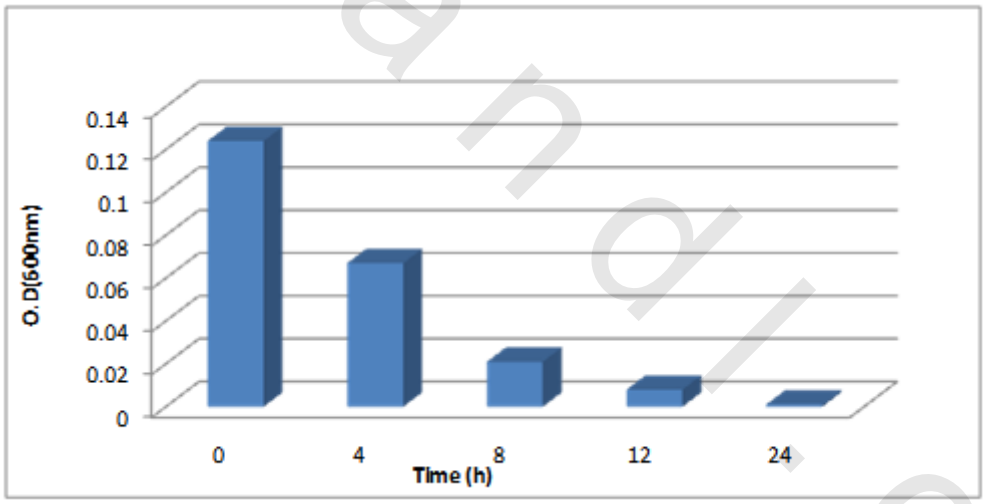

Fig.39: Shows the effect of CA nanofiber loaded with Ag NPs (5w%) on growth kinetic of *E-Coli* though 24 hours.

B- Growth kinetics study for *S. aureus*.

Table (3): Growth kinetics study for *S. aureus* using CA nanofibers loaded with different concentrations of Ag NPs.

Ag w % / Time (hour)	Optical Density (O.D)			
	Control (0%)	1%	3%	5%
0	0.112±0.015	0.112±0.015	0.112±0.015	0.112±0.015
1	0.195±0.017	0.092±0.016	0.071±0.013	0.06±0.014
2	0.26±0.025	0.072±0.015	0.062±0.011	0.054±0.014
3	0.362±0.027	0.061±0.014	0.042±0.012	0.032±0.013
4	0.421±0.021	0.044±0.012	0.03±0.011	0.021±0.012
5	0.433±0.029	0.032±0.015	0.026±0.012	0.018±0.01
6	0.488±0.034	0.03±0.01	0.02±0.001	0.012±0.001

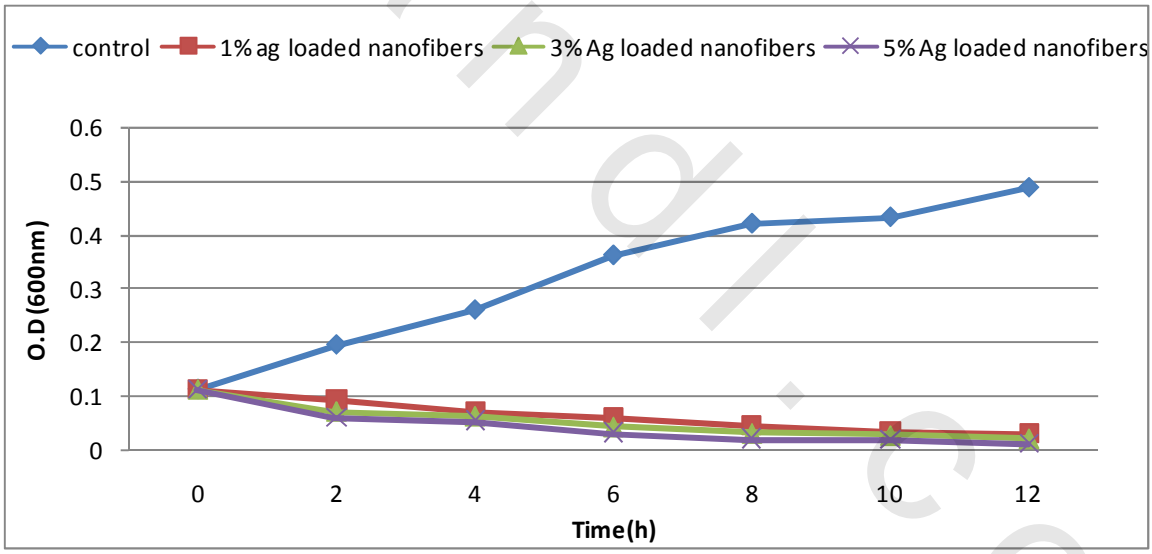

Fig. 40: Effect of Ag coated nanofibers with different concentrations on the growth of *S. aureus*.

Table (4): Zone of Inhibition of Antibacterial Test of CA nanofibers loaded with Ag NP for *S. aureus.*

Ag w%	Zone of Inhibition (cm)
0	0
1	0.95±0.035
3	1.3±0.065
5	1.7±0.072

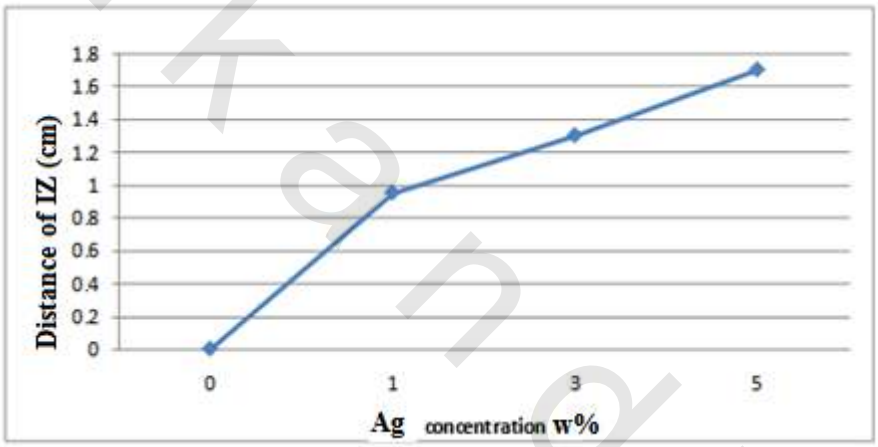

Fig. 41: The effect of different concentration of Ag loaded nanofibers with different concentrations on S. aureus.by plotting the diameter of the inhibition zone of bacterial growth against Ag loaded nanofibers with different concentrations.

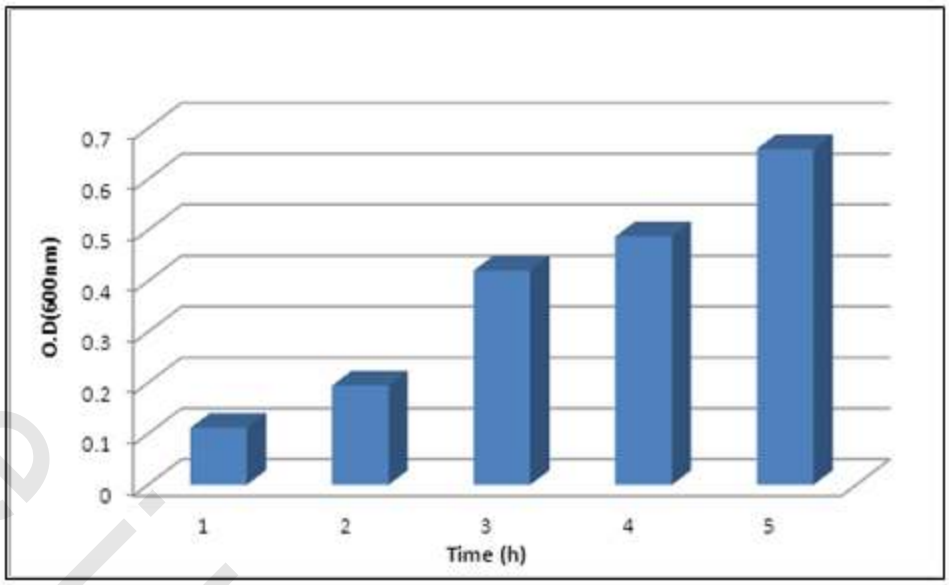

Fig. 42: Shows the effect of CA nanofiber on growth kinetic of *S. aureus* through 24 hours.

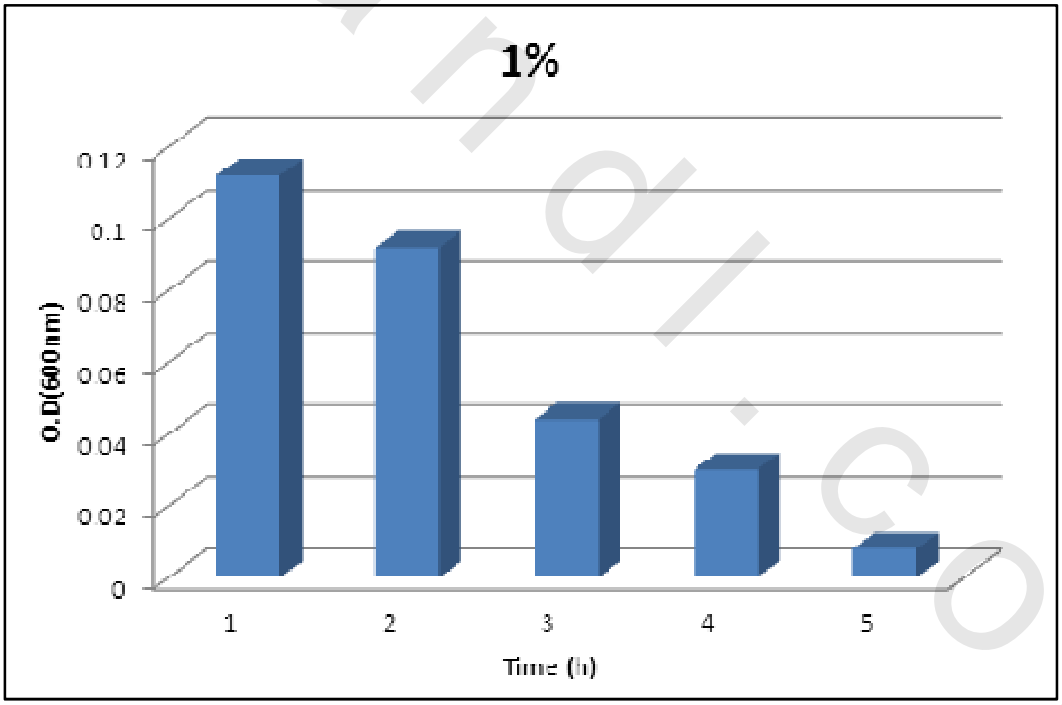

Fig. 43: Shows the effect of CA loaded with (1%) Ag nanoparticles growth kinetic of *S. aureus* through 24 hours.

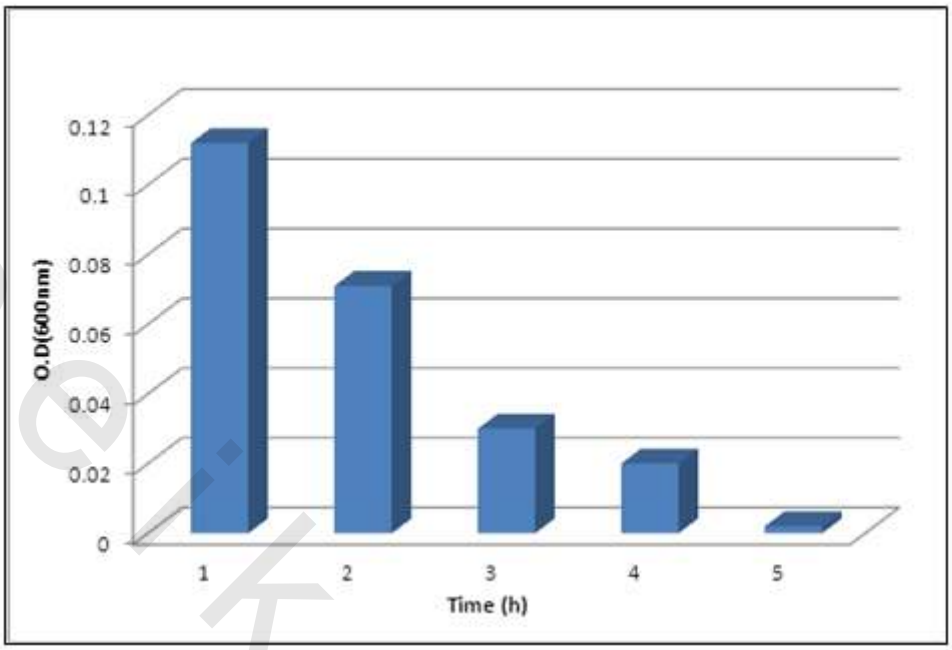

Fig. 44: Shows the effect of CA loaded with (3%) Ag nanoparticles growth kinetic of *S. aureus* through 24 hours.

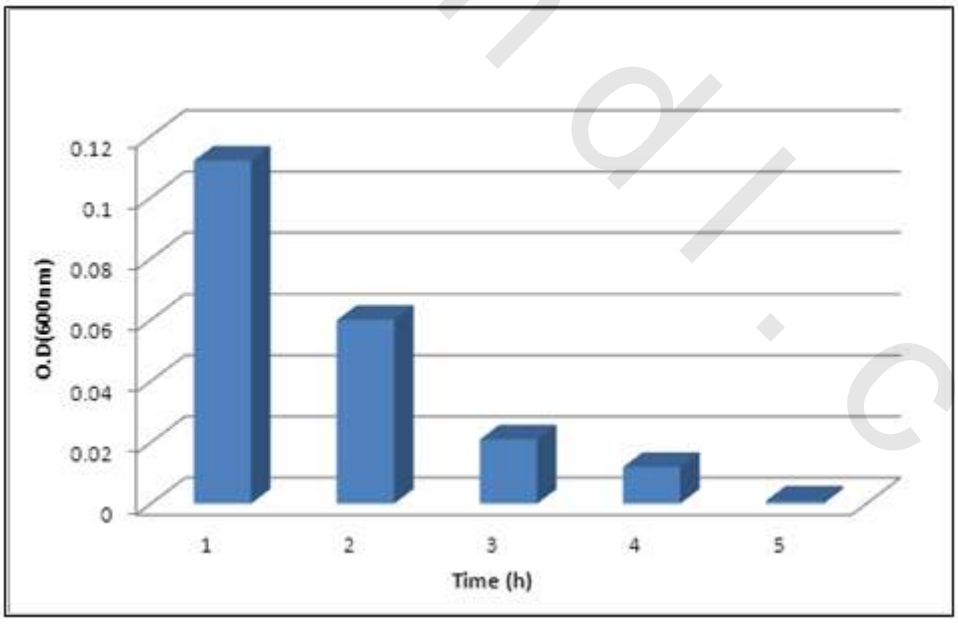

Fig.45: Shows the effect of CA loaded with (5%) Ag nanoparticles growth kinetic of *S. aureus* through 24 hours.

III- Healing Factor

Table (5) and Figure (46) show the relation between healing factor and treatment time of control group and all treated groups through 21 days. Healing factor of different group increases with increasing of the treatment time. Healing factor of the diabetic mice treated with insulin dressed with nanofibers loaded with Ag NPs shows a healing factor higher than that of the normal group.

Table (5): **The healing factor of control and experimental groups treated with different modalities.**

Treatment time (days)	*H.F.* (gp treated with naofiber containing silver)	*H.F.* (gp treated with Laser 5J/cm^2)	*H.F.* (gp treated with silver)	*H.F.* (gp treated with nanofiber)	*H.F.* (gp treated with US 0.5W/cm)	*H.F.* (gp treated with Insulin)	*H.F.* (Control gp.)
1	0	0	0	0	0	0	0
3	56±2.6	50±4.5	45±4.5	39±2.4	39±5.2	32±4.5	45±4.5
5	68±5.2	57±5.2	53±2.6	50±4.5	51±2.6	42±5.2	59±4.5
7	68±5.2	57±5.2	53±2.6	50±4.5	51±2.6	42±5.2	59±4.5
9	77±6.4	66±5.2	60±2.6	57±5.2	60±2.6	53±2.6	63±4.5
11	85±4.3	77±4.5	71±2.6	68±4.5	68±4.5	62±6.9	71±2.6
13	94±2.2	89±2.6	79±6.9	72±4.5	75±2.6	68±4.5	74±2.6
15	100	94±2.9	92±2.6	80±2.6	80±2.6	75±5.2	75±2.6
17	100	100	100	93±2.6	93±2.6	83±2.6	89±2.6
19	100	100	100	100	100	85±2.6	93±2.6
21	100	100	100	100	100	85±2.6	100

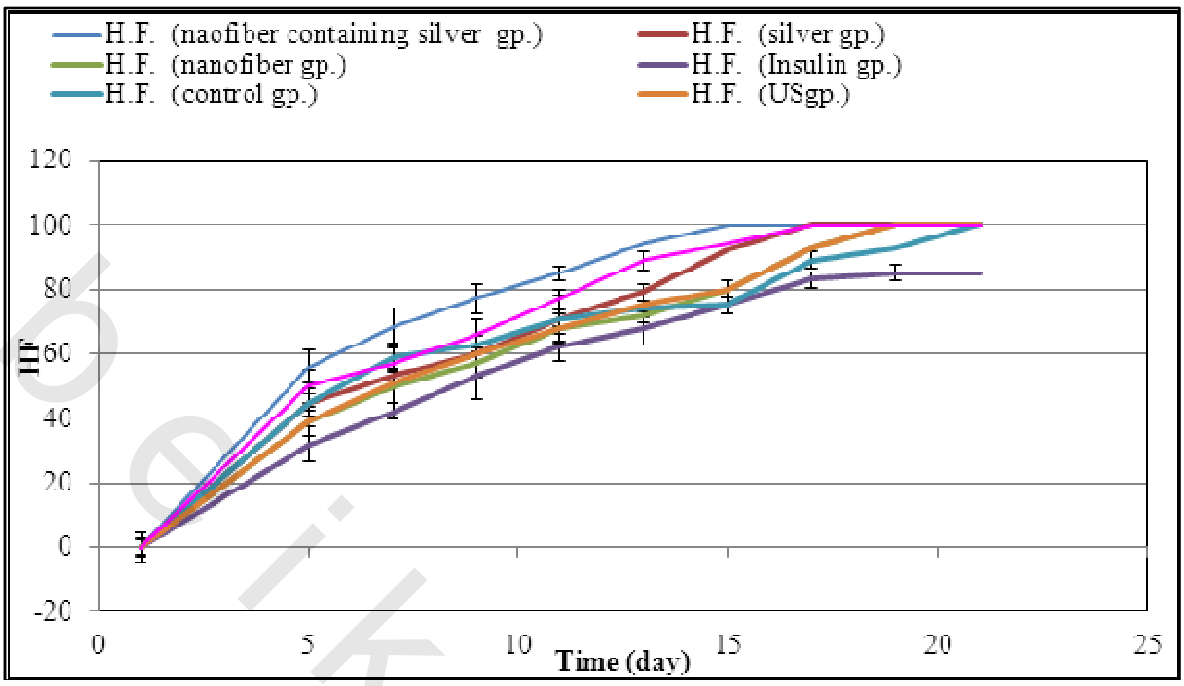

Fig. 46: **The relation between healing factor and treatment period (days) of different groups through 21 days.**

IV- Mechanical properties of healed skin

Mechanical properties of skin of control and experimental groups are shown in Figure (47). It was difficult to measure the mechanical properties of the skin of the untreated diabetic mice because their skin was brittle. Wound dressing using nanofibers loaded with Ag NPs improve the skin wound healing and the mechanical properties of the treated skin of the diabetic mice.

Marked improvement in wound strength and healing due to increase in formation of collagen fibers and activity of the epithelial covering in mice receiving STZ and treated with insulin in combination with dressing with nanofibers loaded with Ag NPs.

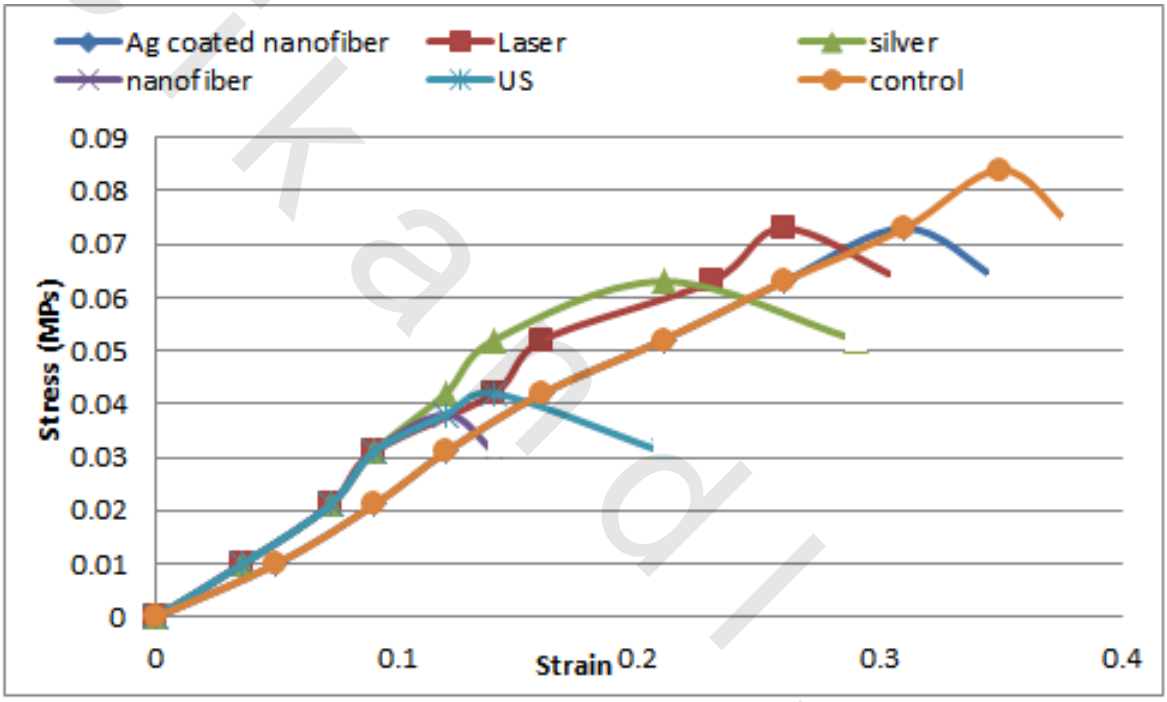

Fig. 47: Stress-strain curve of the skin of control and diabetic mice treated with different modalities.

V- Histopatholgical Examination of mice skin during period of healing

Histopathological examination of the healed skin was performed at 4th, 10 th and 15 th days of treatment as shown in Figures (49-66) in comparison with control skin (Figure 48).

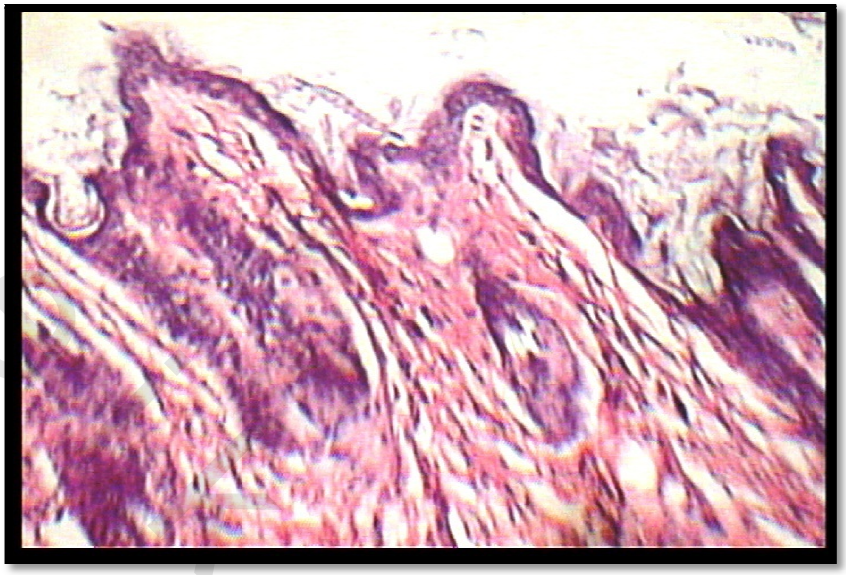

Fig. 48: Cutaneous sample of a control mouse showing normal epithelium and subepithelial collagen fiber (H&E stain x100).

1- At the 4th day

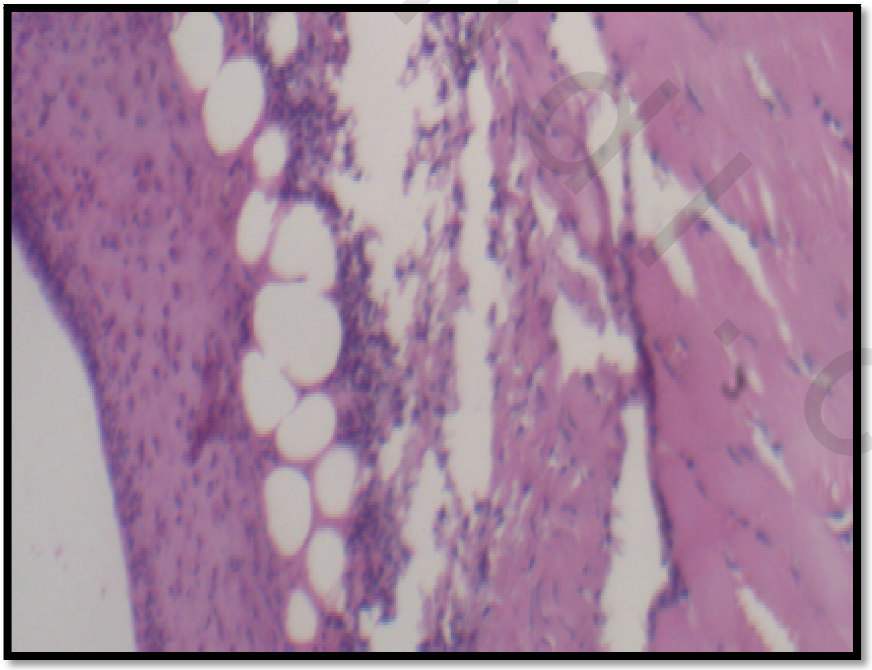

Fig. 49: Cutaneous sample diabetic induced mice at 4th day of treatment, wound treated with insulin and Ag loaded ,shows complete ulceration of the surface epithelium that replaced by proliferating collagen, fibrous tissue deposition, moderate inflammatory cellular infiltrate, hemorrhage and edema (H&E x400).

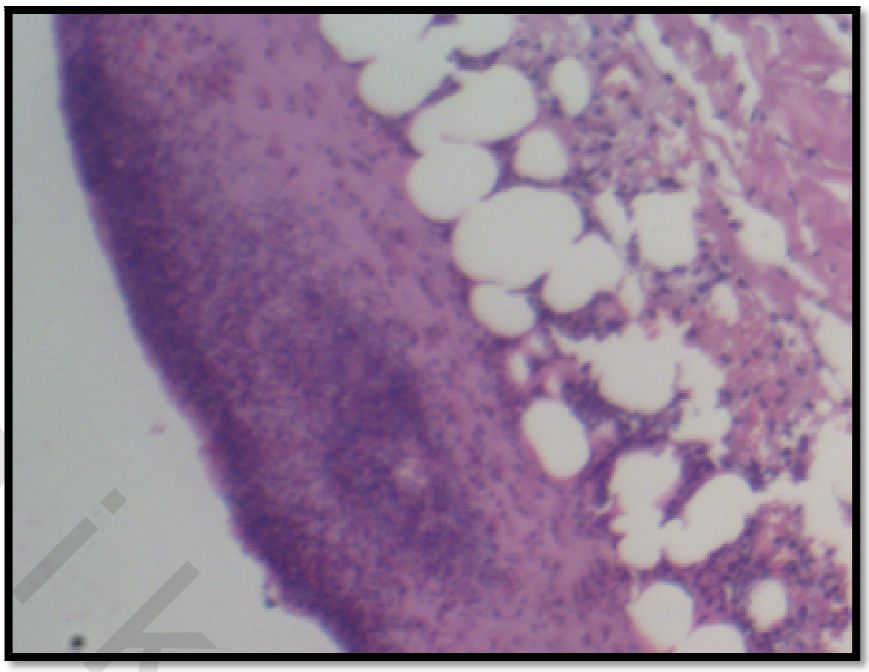

Fig. 50: **Cutaneous sample diabetic induced mice at 4th day of treatment, wound treated with insulin and Laser shows complete ulceration of the surface epithelium, moderate inflammatory infiltrate that involves the subcutaneous fat. (H&E x40).**

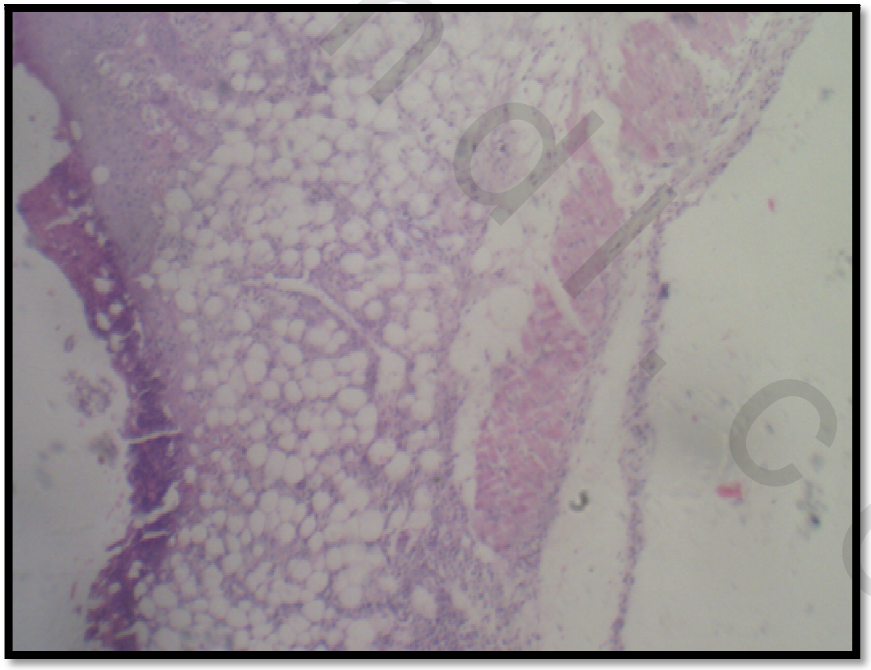

Fig. 51: **Photomicrography of mice skin of diabetic induction at 4th day of treatment with insulin and Ag NPs showing complete ulceration of surface epithelium that covered by fibrinoid material infiltrated by inflammatory cells and moderate collagen deposition. (H&E x40).**

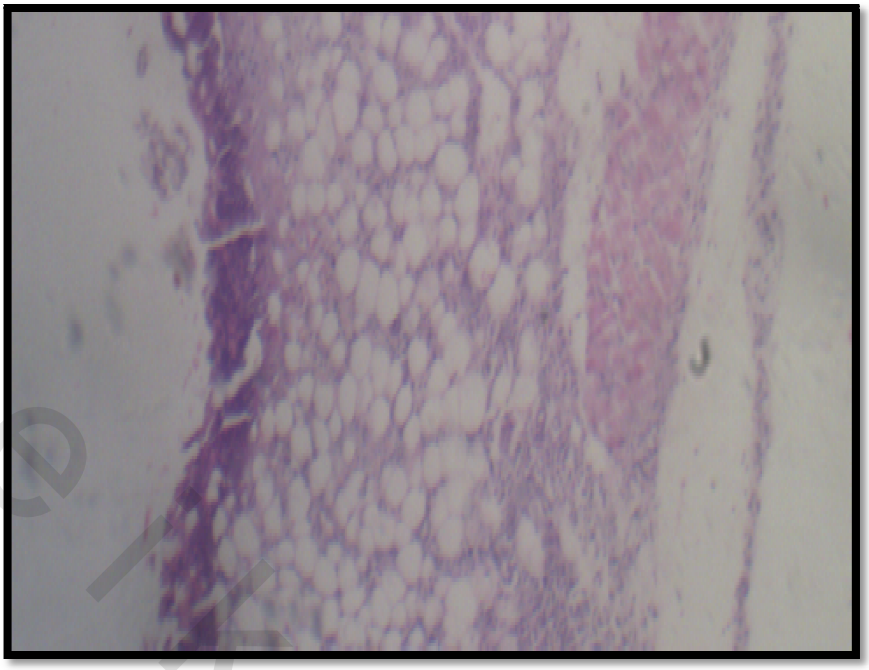

Fig. 52: **Photomicrography of mice skin of diabetic induction at 4th day of treatment with insulin and and either nanofiber or US showing complete ulceration of surface epithelium that covered by fibrinoid material infiltrated by inflammatory cells and moderate collagen deposition. (H&E x40).**

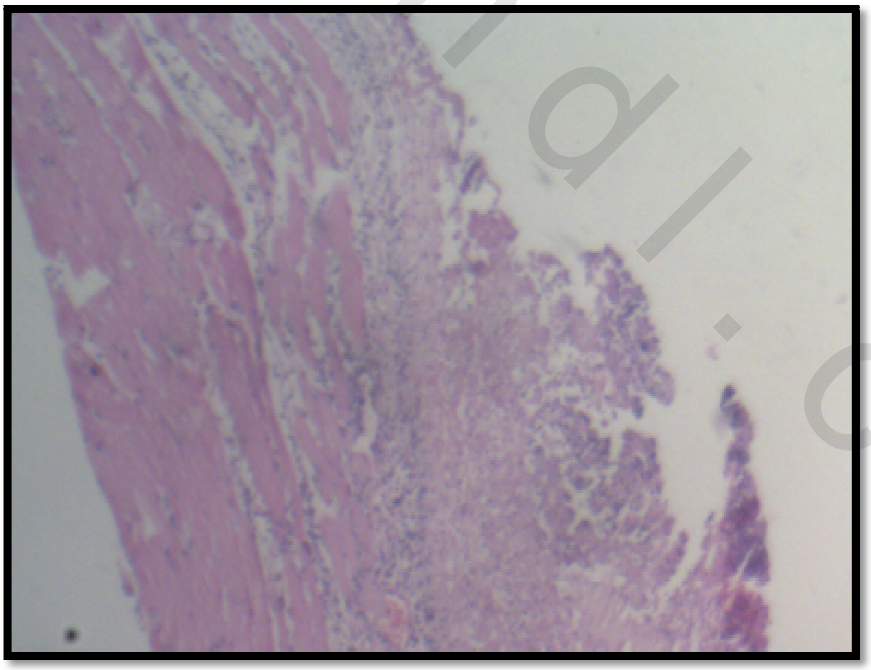

Fig. 53: **Photomicrography of diabetic mice skin at 4th day of treatment with insulin showing complete ulceration of surface epithelium, moderate collagen deposition and inflammatory cells infiltrate. (H&E x40).**

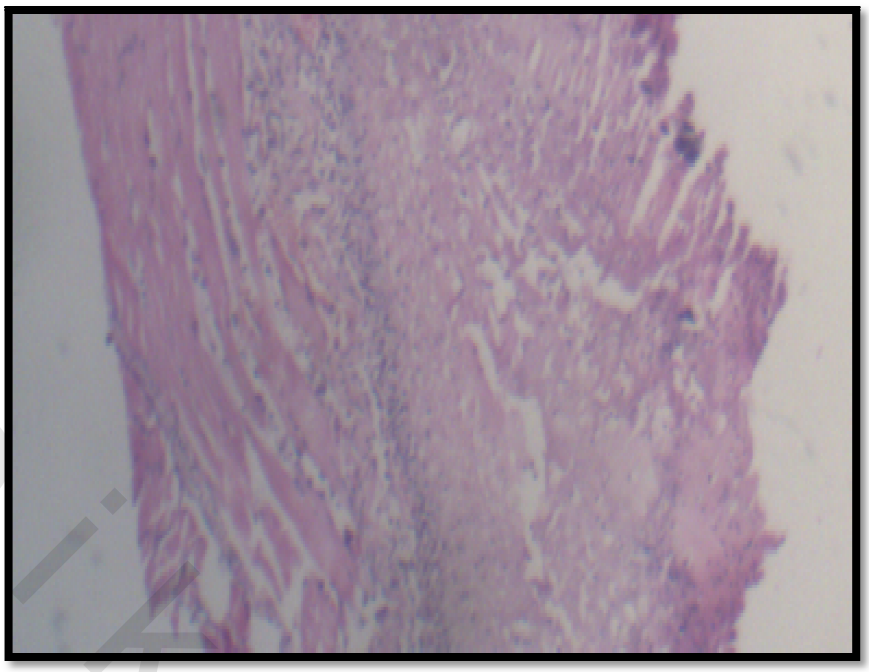

Fig. 54: **Photomicrography of mice skin in control (diabetic free mice) at 4th day showing complete ulceration of surface epithelium and moderate collagen deposition. (H&E x40).**

2- At 10th day

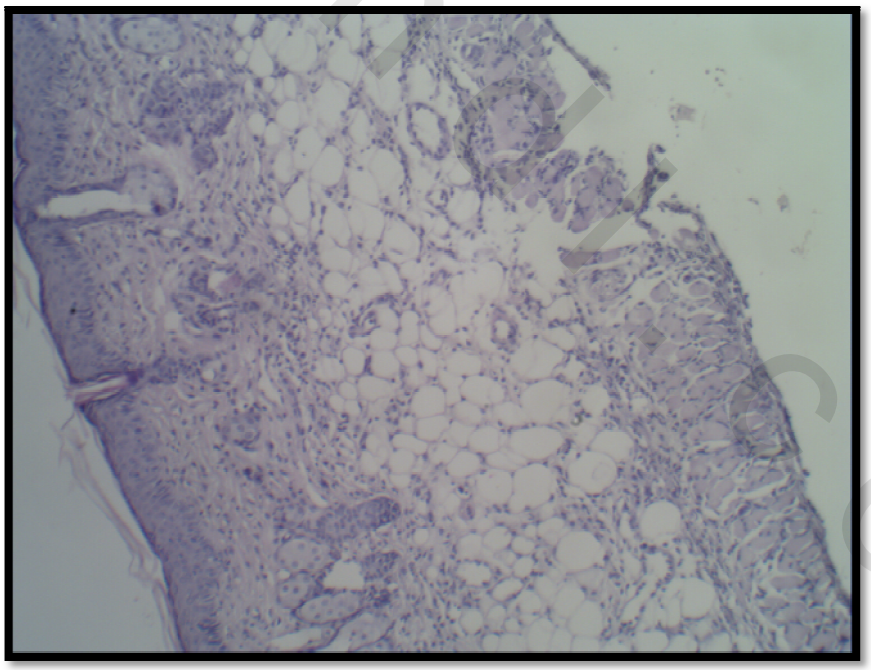

Fig. 55 : **Cutaneous sample of mice skin of diabetic induction at 10th day of treatment with insulin and Ag loaded nanofiber showing intact skin with normal maturation sequence, the collagen deposition in upper and mid dermis and mild inflammatory cellular infiltrate. (H&E x40).**

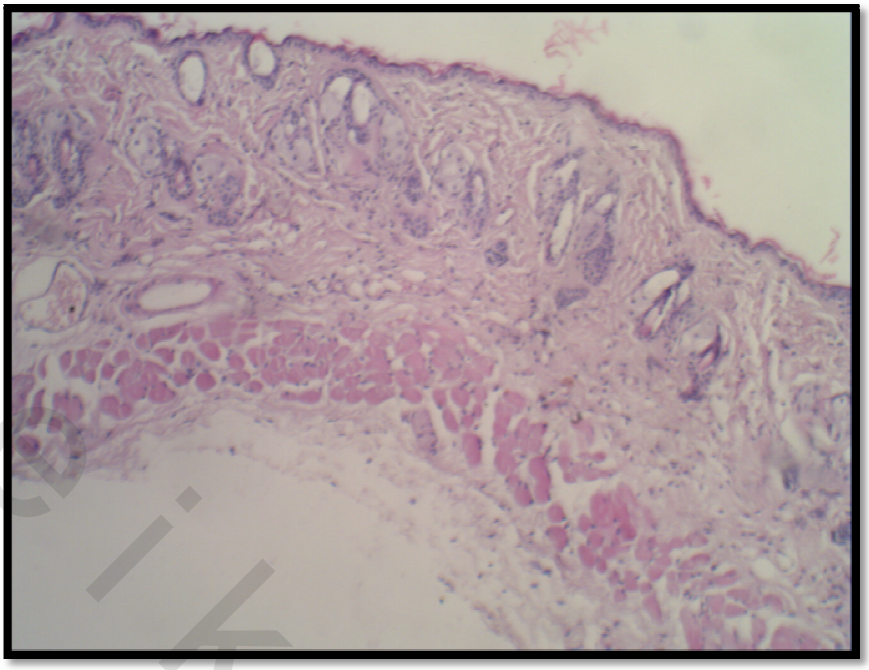

Fig. 56: **Cutaneous sample of mice skin of diabetic induction at 10th day of treatment with insulin and laser showing intact thinned epidermis with normal maturation sequence of the epithelium.(H&E x40).**

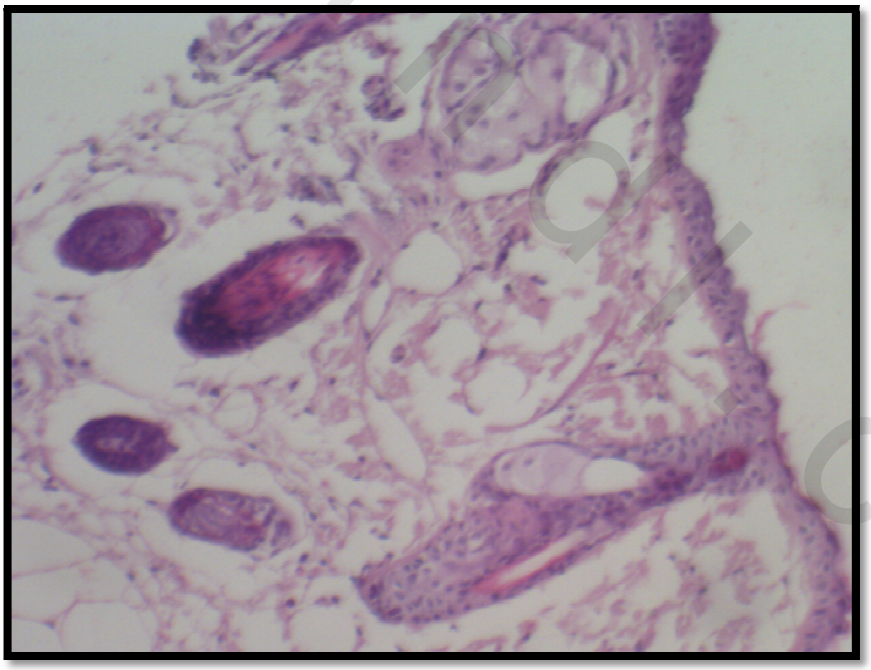

Fig. 57: **Photomicrography of mice skin of diabetic induction at 10th day of treatment with insulin and Ag NPs showing midly atrophic skin, the dermis is showing edema and mild collagen deposition.(H&E x40).**

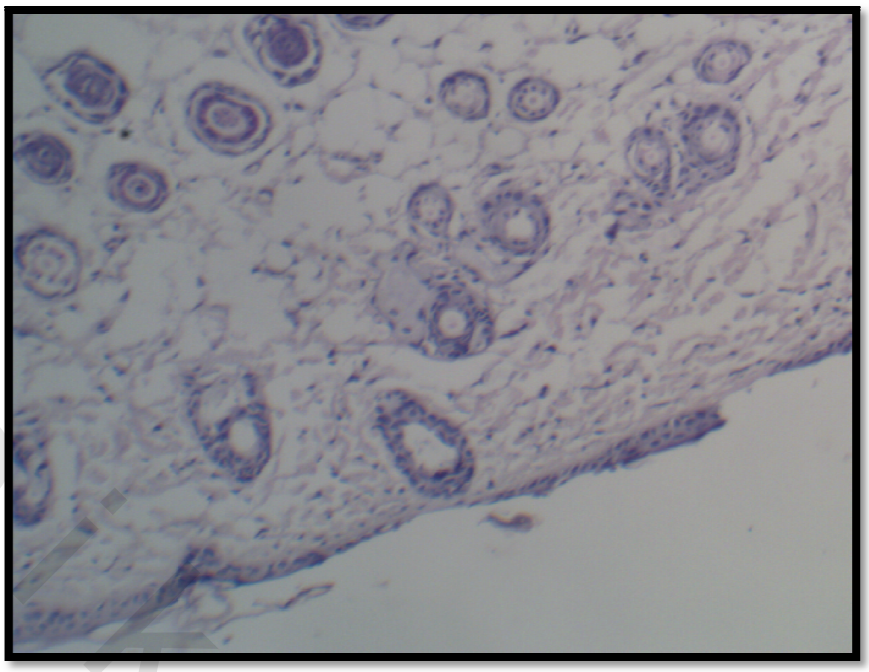

Fig. 58: **Photomicrography of mice skin of diabetic induction at 10th day of treatment insulin and either nanofiber or US demonstrating skin with focal epidermal ulceration, thinning and the minimal collagen deposition.(H&E x40).**

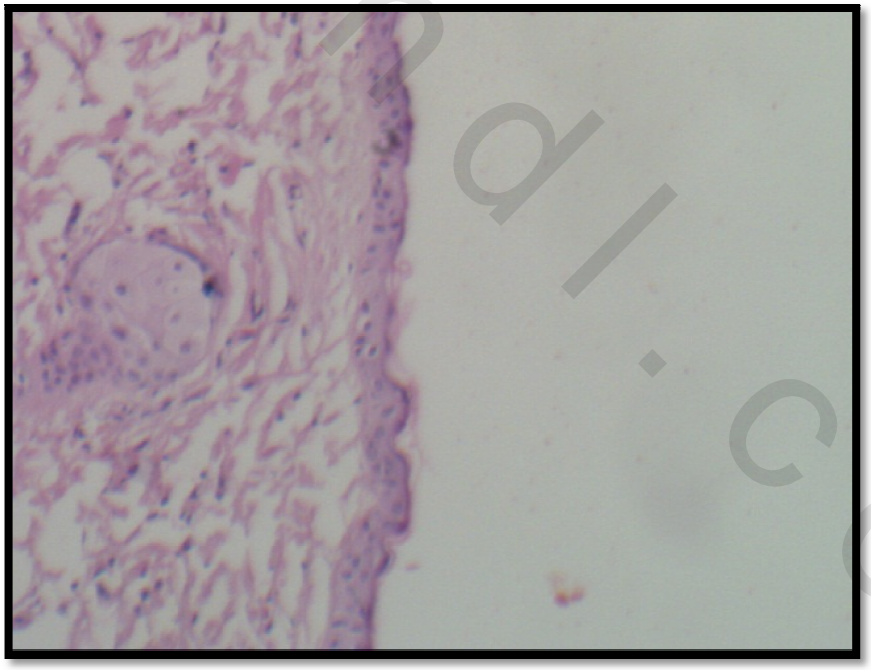

Fig. 59: **Photomicrography of mice skin ,diabetic induction at 10th day of treatment with insulin showing thinning of the skin epidermis, the collagen is disrupted with edematous areas, (H&E x40).**

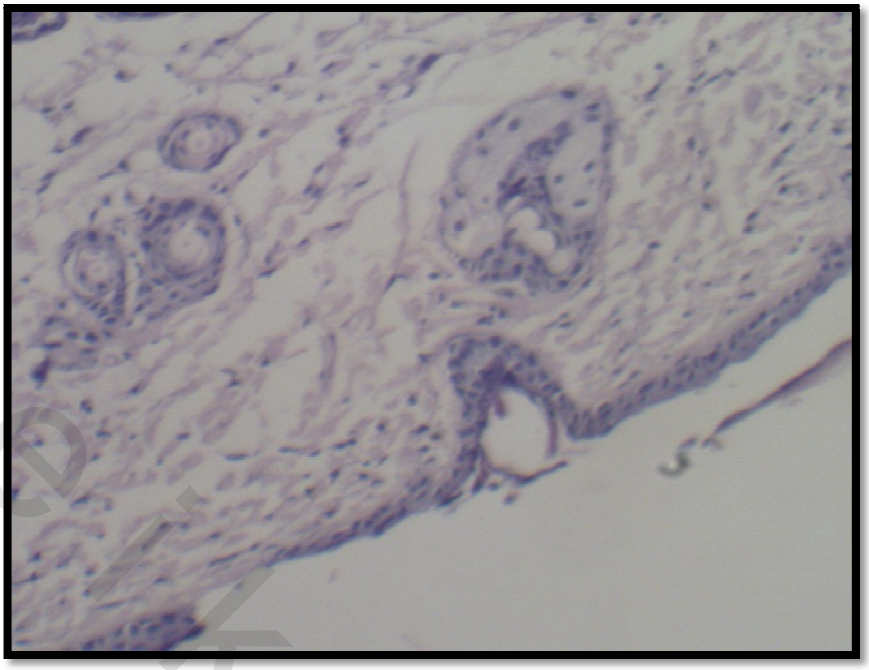

Fig. 60: **Photomicrography of mice skin in control (diabetic free mice) at 10th day showing focal ulceration, minimal edema and moderate collagen deposition.(H&E x40).**

3- After 15 days

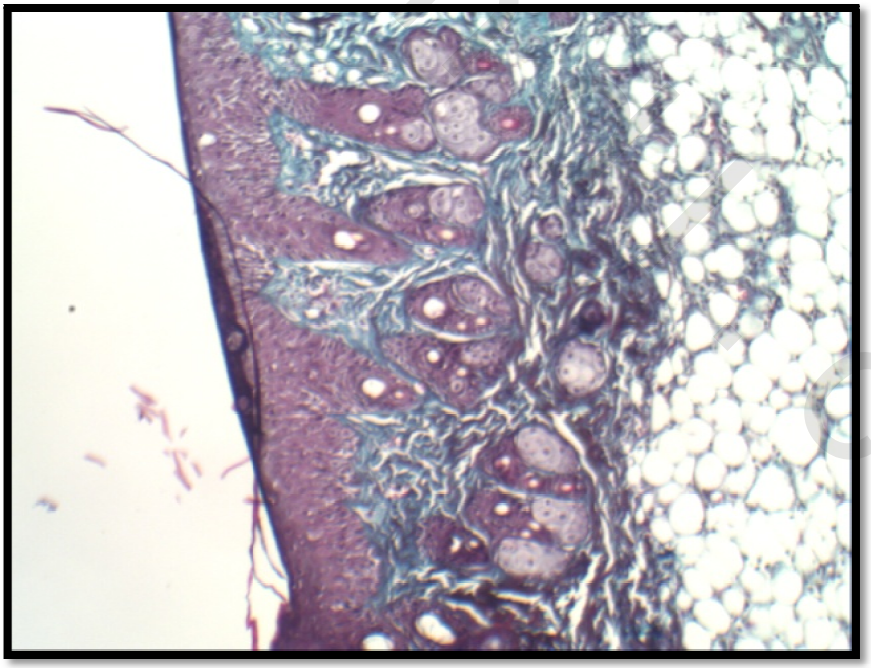

Fig. 61: **Photomicrography of mice skin of diabetic induction at 15th day of treatment with insulin and Ag loaded nanofiber showing intact skin covering with dense collagen deposition.(Masson trichromex40).**

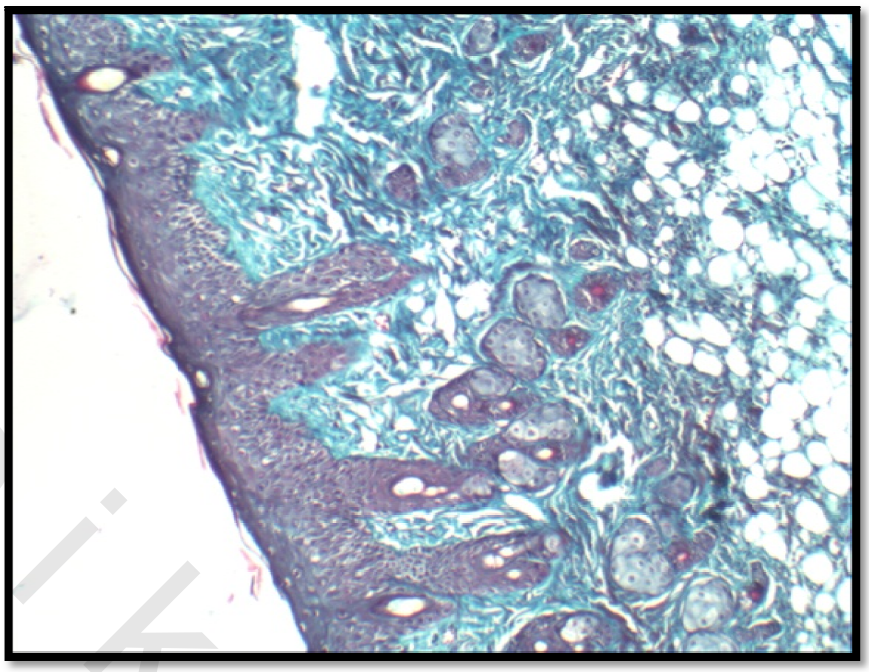

Fig. 62: **Photomicrography of mice skin of diabetic induction at 15th day of treatment with insulin and laser to demonstrate intact skin with normal maturation sequence of the epithelium, the collagen is abundant with mild fibroblastic proliferation.(Masson trichromex40).**

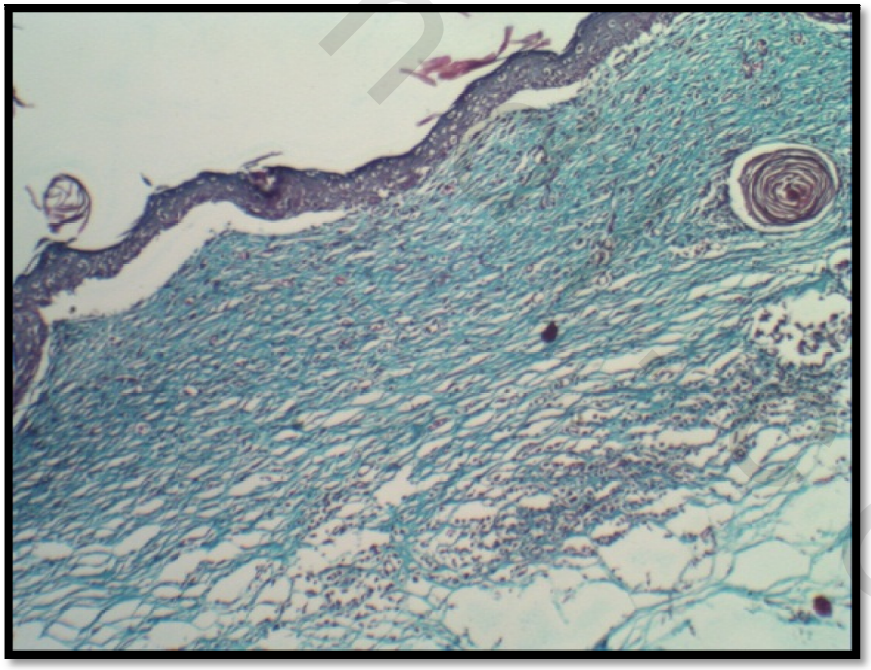

Fig. 63: **Photomicrography of mice skin of diabetic induction at 15th day of treatment with insulin and Ag NPs showing well-formed epithelial covering with focal atrophy and absence of rete ridges, prominent collagenic and fibroblastic proliferation.(Masson trichromex40).**

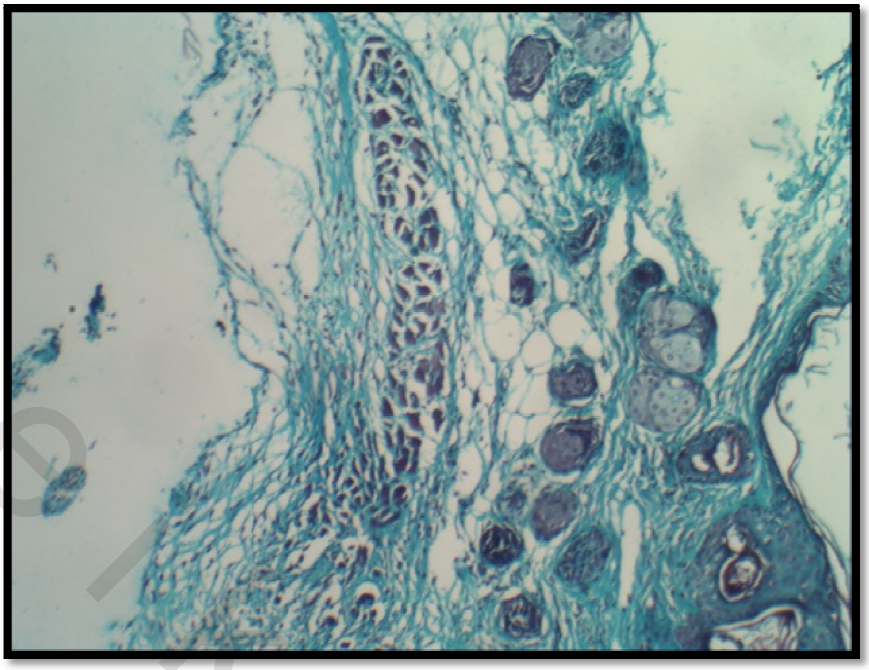

Fig. 64: **Photomicrography of mice skin of diabetic induction at 15th day of treatment with insulin and either nanofiber or US to demonstrate focal skin ulceration and focal intact area of the lining epithelium and moderate collagen deposition particularly in the upper dermis. (Masson trichromex40).**

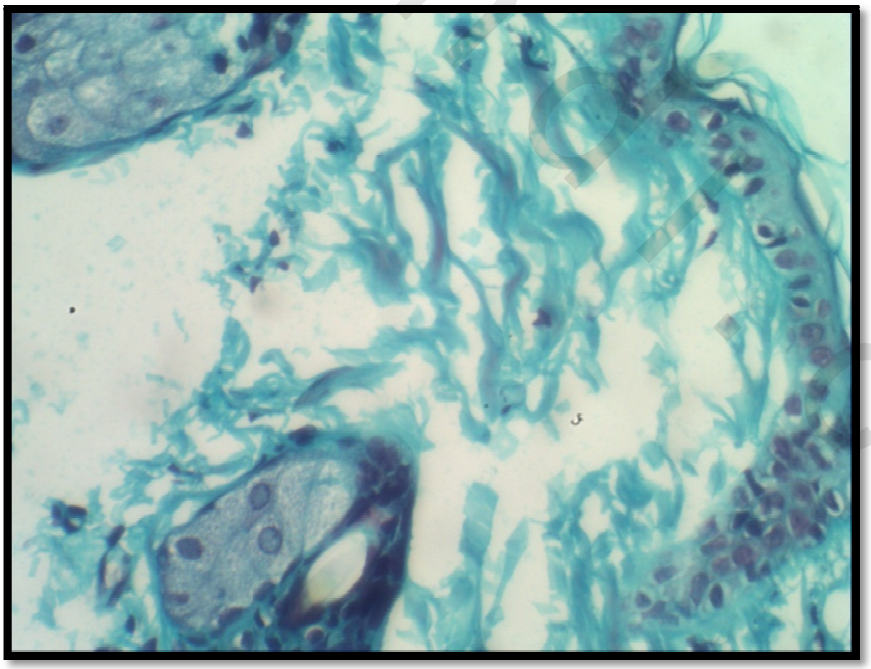

Fig. 65: **Photomicrography of diabetic mice skin at 15th day of treatment with insulin showing thinning of the epithelium, the collagen is disrupted with edematous areas. (Masson trichromex40).**

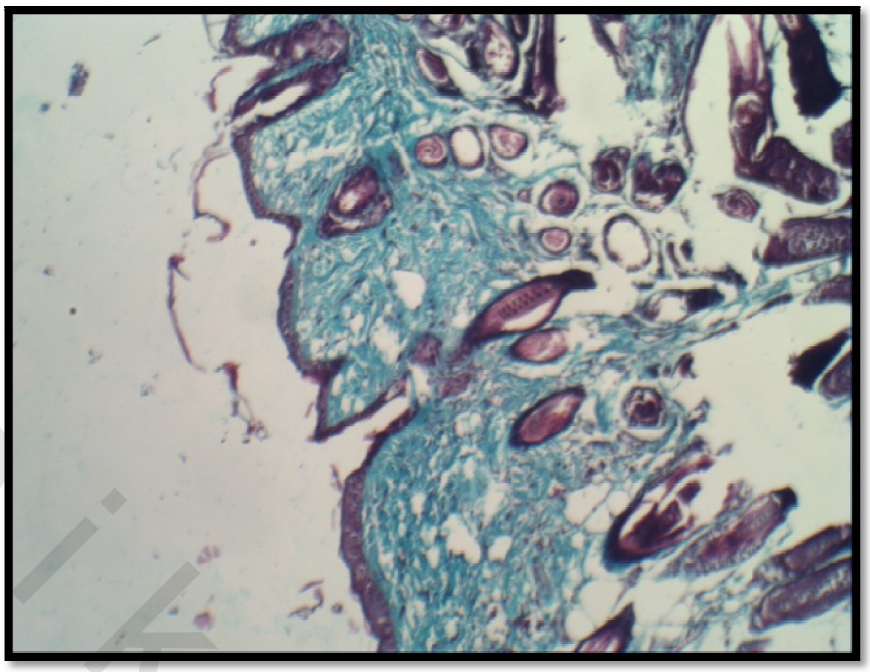

Fig. 66: **Photomicrography of mice skin in control (diabetic free mice) at 15th day showing focal ulceration of the epithelium, the collagen is dense in the upper dermis.(Masson trichromex40).**